Atmos. Chem. Phys. Discuss., 15, 21607–21669, 2015
www.atmos-chem-phys-discuss.net/15/21607/2015/
doi:10.5194/acpd-15-21607-2015

Atmospheric Chemistry and Physics Discussions
Open Access

Size distribution and optical properties of mineral dust aerosols transported in the western Mediterranean

C. Denjean[1,2], F. Cassola[3], A. Mazzino[3], S. Triquet[1], S. Chevaillier[1], N. Grand[1], T. Bourrianne[4], G. Momboisse[4], K. Sellegri[5], A. Schwarzenbock[5], E. Freney[5], M. Mallet[6], and P. Formenti[1]

[1]Laboratoire Interuniversitaire des Systèmes Atmosphériques (LISA), UMR-CNRS 7583, Université Paris-Est-Créteil (UPEC) et Université Paris Diderot (UPD), Institut Pierre Simon Laplace (IPSL), Créteil, France
[2]Leibniz Institute for Tropospheric Research (TROPOS), Permoserstraße 15, 04318, Leipzig, Germany
[3]Department of Physics and INFN, Genoa, Italy
[4]Centre National de Recherches Météorologiques (CNRM), Météo-France, Toulouse, France
[5]Laboratoire de Météorologie Physique (LaMP), CNRS/Université Blaise Pascal, Clermont-Ferrand, France
[6]Laboratoire d'Aérologie (LA), Université de Toulouse, CNRS, Toulouse, France

Received: 9 July 2015 – Accepted: 22 July 2015 – Published: 10 August 2015

Correspondence to: C. Denjean (denjean@tropos.de)
and P. Formenti (paola.formenti@lisa.u-pec.fr)

Published by Copernicus Publications on behalf of the European Geosciences Union.

ACPD
15, 21607–21669, 2015

Abstract

This study presents in situ aircraft measurements of Saharan mineral dust transported over the western Mediterranean basin in June–July 2013 during the ChArMEx/ADRIMED (the Chemistry-Aerosol Mediterranean Experiment/Aerosol Direct Radiative Impact on the regional climate in the MEDiterranean region) airborne campaign. Dust events differing in terms of source region (Algeria, Tunisia and Morocco), time of tranport (1–5 days) and height of transport were sampled. Mineral dust were transported above the marine boundary layer, which conversely was dominated by pollution and marine aerosols. The dust vertical structure was extremely variable and characterized by either a single layer or a more complex and stratified structure with layers originating from different source regions. Mixing of mineral dust with pollution particles was observed depending on the height of transport of the dust layers. Dust layers carried higher concentration of pollution particles at intermediate altitude (1–3 km) than at elevated altitude (> 3 km), resulting in scattering Angstrom exponent up to 2.2 within the intermediate altitude. However, the optical properties of the dust plumes remained practically unchanged with respect to values previously measured over source regions, regardless of the altitude. Moderate light absorption of the dust plumes was observed with values of aerosol single scattering albedo at 530 nm ranging from 0.90 to 1.00 ± 0.04. Concurrent calculations from the aerosol chemical composition revealed a negligible contribution of pollution particles to the absorption properties of the dust plumes that was due to a low contribution of refractory black carbon in regards to the fraction of dust and sulfate particles. This suggests that, even in the presence of moderate pollution, likely a persistent feature in the Mediterranean, the optical properties of the dust plumes could be assimilated to those of native dust in radiative transfer simulations, modeling studies and satellite retrievals over the Mediterranean. Measurements also showed that the coarse mode of mineral dust was conserved even after 5 days of transport in the Mediterranean, which contrasts with the gravitational depletion of large particles observed during the transport of dust plumes over the At-

ACPD
15, 21607–21669, 2015

lantic. Simulations with the WRF mesoscale meteorological model highlighted a strong vertical turbulence within the dust layers that could prevent deposition of large particles during their atmospheric transport. This has important implications for the dust radiative effects due to surface dimming, atmospheric heating and cloud formation. The results presented here add to the observational dataset necessary for evaluating the role of mineral dust on the regional climate and rainfall patterns in the western Mediterranean basin.

1 Introduction

Mineral dust aerosols constitute a major fraction of airborne particulate matter (Huneeus et al., 2012) and their contribution to the Earth's climate system is of considerable significance. In particular, dust aerosols exert a significant effect on global radiative budget by scattering and absorbing longwave and shortwave radiation (IPCC, 2013), thereby impacting the vertical profile of temperature and atmospheric stability (Jing et al., 2008) and the precipitation rate (Rosenfeld et al., 2001; Andreae and Rosenfeld, 2008; Choobari et al., 2014).

The Sahara desert hosts the maximum dust emission and atmospheric dust loading in the world (Choobari et al., 2014). Strong winds and convection produced by intense surface heating can uplift mineral dust particles into the free troposphere, where they are advected over large distances at the continental and intercontinental scales (d'Almeida, 1986; Goudie and Middleton, 2001; Engelstaedter et al., 2006). Along the year, the transport pathway of Saharan dust is mainly controlled by low-pressure systems over the Atlantic or North Africa, high pressure over the Mediterranean region, or high pressure at upper level over Africa (Moulin et al., 1998; Querol et al., 2009; Salvador et al., 2014). A significant fraction of dust loaded from Africa sources are transported westward across the Atlantic Ocean as far as the Caribbean (Maring et al., 2003; Doherty et al., 2008), the United States (Perry et al., 1997; Prospero et al., 2002) and South America (Swap et al., 1992; Formenti et al., 2001; Ansmann et al., 2009).

ACPD
15, 21607–21669, 2015

Large Saharan dust storms are also carried across the Mediterranean Sea to Europe (Moulin et al., 1998; Koren et al., 2003; Collaud Coen et al., 2004; Papayannis et al., 2008). During such outbreaks, mineral dust emerges as the largest PM_{10} source at rural and urban sites in the Mediterranean basin (Pey et al., 2013; Salvador et al., 2014).

Considerable uncertainties in quantifying the climatic effect of mineral dust arise from a lack of knowledge of their properties and spatial and vertical distributions over many regions of the world. In particular, to estimate the magnitude of the dust radiative effect, an accurate description of both particle size distribution and optical properties and their link with the chemical composition is necessary (Sokolik and Toon, 1996; Tegen et al., 1996). The size distribution is a fundamental parameter to estimate the aerosol radiative effect and atmospheric lifetime, but its representation remains challenging due to the large size spectrum of mineral dust, from hundreds of nanometers to tenths of micrometers (Formenti et al., 2011a). In particular, an accurate description of the coarse mode particles is vital since the presence of large particles enhance the capacity of mineral dust in absorbing radiation at short and long wavelengths (McConnell et al., 2008; Otto et al., 2009; Sicard et al., 2014), modify the atmospheric heating rate (Ryder et al., 2013a) and affect cloud formation (Koehler et al., 2009).

Once in the atmosphere, mineral dust can undergo various aging processes, such as heterogeneous reactions with gas-phase compounds (Sullivan and Weber, 2006; Ma et al., 2012), condensation of low-volatile species (Clarke et al., 2004; Sullivan and Prather, 2007), cloud processing (Levin et al., 1996; Trochkine et al., 2003) and coagulation (Fan et al., 1996; Zhou et al., 1996; Levin et al., 2005). Because of these processes, the physico-chemical properties (composition, mixing state, shape, and size distribution) of dust aerosols might evolve during transport, leading in turn to the evolution of the optical properties (Formenti et al., 2011a). A recent study of Kanitz et al. (2014) has shown significant differences in the optical properties of two Saharan dust plumes over the Atlantic Ocean, resulting from different aging processes affecting the dust. Henceforth, the radiative effect of mineral dust should depend on the travel

ACPD
15, 21607–21669, 2015

distance and pathway, residence time over their source regions and air masses encountered (Garrett et al., 2003).

The Mediterranean basin provides ideal conditions to investigate the changes in Saharan dust properties as numerous concurrent anthropogenic and natural sources of aerosols are active over this region. Case studies of mixing of Saharan dust with industrial/urban, marine and biomass burning particles have been documented in the past (Koçak et al., 2012; Mantas et al., 2014), and could explain the large variability of the values of single scattering albedo ω_0 (0.83–0.92 at the wavelength of 440 nm) reported by various studies (Sicard et al., 2012; Mallet et al., 2013).

In past years, intensive field campaigns including in situ airborne measurements have mostly focused on properties of mineral dust at emission (e.g., over the Saharan and the Sahelian source regions) and over the Atlantic Ocean, and their comparison to trace the temporal evolution during transport (Formenti et al., 2003, 2011b; Reid et al., 2003; McConnell et al., 2008; Osborne et al., 2008; Heintzenberg, 2009; Weinzierl et al., 2009, 2011; Haywood et al., 2011; Ryder et al., 2013a, b). On the contrary, observations in the Mediterranean region were mostly limited to remote sensing from the ground (e.g. Moulin et al., 1997; Hamonou et al., 1999; Meloni et al., 2006; Saha et al., 2008; Basart et al., 2009; Gómez-Amo et al., 2011; Perrone and Bergamo, 2011; Mallet et al., 2013; Pey et al., 2013; Marconi et al., 2014) or spaceborne (de Meij and Lelieveld, 2011; Gkikas et al., 2012).

To fill this gap, the Aerosol Direct Radiative Impact on the regional climate in the MEDiterranean region (ADRIMED) field campaign, part of the international cooperative research program ChArMEx (the Chemistry-Aerosol Mediterranean Experiment; http://charmex.lsce.ipsl.fr) took place with the main objectives of characterizing Saharan dust plumes by coordinated aircraft and ground-based measurements (Mallet et al., 2015). In this paper, we present in situ aircraft measurements obtained in June–July 2013 over the Mediterranean basin. The objective is to determine possible changes of dust properties during long-range transport over the western Mediterranean basin and explore the potential reasons for changes. Particle size distribution, chemical

ACPD
15, 21607–21669, 2015

composition and the associated optical properties are presented, and their variability due to altitude and dust age are discussed.

2 Measurement and methodology

2.1 Aircraft strategy

The ATR-42 aircraft of SAFIRE (French aircraft service for environmental research, http://www.safire.fr) based at Cagliari (39°15′ N, 9°03′ E, Italy) conducted 16 flights in the period 14 June–4 July 2013. In this paper, we present results from the 9 flights dedicated to the observation of mineral dust plumes that occurred between 16 June and 3 July 2013. The ATR-42 aircraft performed research flights in the area between 35 to 43° N and −4 to 13° E, covering the western Mediterranean region to probe the Saharan dust properties in a range of varying transport pathways and source regions. The flight tracks are shown in Fig. 1 and a summary of flight information is provided in Table 1.

The airborne missions were planned using four different dust plume forecast models (MACC ALADIN-Dust, SKIRON and BSC-DREAM8b v2.0) and satellite images from the SEVIRI radiometer on the Meteosat Second Generation (MSG) satellite, all available in real time from the ChArMex Operating Center (http://choc.sedoo.fr/) during the campaign. The general weather forecast was made daily by the French school of Meteorology (ENM), at Météo-France in Toulouse.

The general flight strategy consisted of two main parts: first, profiles from 300 m up to 6 km a.s.l. were conducted to sound the vertical structure of the atmosphere and identify interesting dust layers. Afterwards, the identified dust layers were probed by straight levelled runs (SLR), where the aircraft flew at fixed altitudes, to provide information on dust spatial variability and properties. Horizontal flight legs in the dust layers lasted 20–40 min to allow aerosol collection on filters. At the typical aircraft cruise speed of 100 m s^{-1}, samples had spatial resolution ranging from 121 to 242 km.

ACPD
15, 21607–21669, 2015

2.2 Instrumentation

The ATR-42 basic instrumentation provides meteorological parameters including temperature, dew point temperature, pressure, turbulence, relative humidity, wind speed, direction, CO and O_3 concentrations (Saïd et al., 2010). Only instruments relevant to microphysical properties, chemical composition and optical properties of aerosols are detailed in Table 2.

2.2.1 Aerosol concentration and size distribution

The total number concentration of particles larger than 5 nm in diameter was measured using a butanol-based condensation nucleus counter (CPC, TSI model 3075) corrected for coincidences.

The particle number size distribution was measured over the largest possible size spectrum by combining optical and electrical mobility techniques.

The number size distribution in the submicron range was measured with an in-cabin Scanning Mobility Particle Sizer (SMPS) and a wing-mounted Ultra High Sensitivity Aerosol Spectrometer (UHSAS, Droplet Measument Technologies). The SMPS consisted of a Differential Mobility Analyzer (DMA, Villani et al., 2007) interfaced to a Condensation Particle Counter (CPC, TSI model 3010). A closed-loop recirculation was used for the sheath flow of the DMA. The SMPS system provided the number size distribution of the electrical mobility diameter from the 30–400 nm in 135 nominal size classes over time scans lasting 120 s. Therefore, only data acquired during SLR are considered. Data were processed by taking into account the particle electrical charging probabilities, the CPC counting efficiencies, the DMA transfer functions and the diffusion losses in the SMPS and CPC systems. The UHSAS is an optical-scattering laser-based aerosol spectrometer, providing the number size distribution of the optical equivalent diameter from 0.04 to 1 µm in 99 nominal size classes at a time resolution of 1 s. The spectrometer integrates light scattering between 22 to 158° at 1054 nm. Due to reduced counting efficiency at size larger than 0.9 µm, only data at lower sizes are

ACPD
15, 21607–21669, 2015

considered in this paper. The uncertainties on the particle diameter were estimated to be 5 and 10 % for the SMPS and UHSAS, respectively (Wiedensohler et al., 2012; Cai et al., 2008).

The number size distribution in the supermicron range was measured by the combination of two different optical particle counters (OPC). A wing-mounted Forward Scattering Spectrometer Probe (FSSP, Particle Measuring System, Model 300) measured the optical size distribution in the nominal size range of 0.28 to 20 µm (Baumgardner et al., 1992). Data were recorded in 30 size classes at 1 s interval. The FSSP-300 is based on the measurement of the light scattered between 3 and 12° at 632.8 nm. Possible errors in the FSSP-300 sizing were assumed to be 30 % of the particle diameter according to Baumgardner et al. (1992). A GRIMM OPC (model sky-OPC 1.129) operated inside the cabin at a 6 s time resolution and measuring the optical size distributions between 0.3 and 32 µm on 32 size classes in nominal diameter. The instrument integrates light scattering between 30 and 150° at 655 nm. According to the calibration of the GRIMM with standard, we assumed 10 % uncertainties in particle sizing.

2.2.2 Aerosol chemical composition

Bulk aerosol samples were collected on-board by filtration through two stainless-steel filter units mounted in parallel. Sampling was performed only during constant altitude sequences lasting more than 25 min in order to guarantee sufficient mass loading of the filter samples. After exposure, samples were stored and transported at −20 °C to avoid later modification. Once in the laboratory, samples collected on 42 mm diameter polycarbonate membranes (nominal pore size 0.4 µm Nuclepore, Whatman) were cut in halves that were analyzed to yield the elemental and ionic composition. Concentrations of elements from Na to Pb were measured by wavelength-dispersive X–ray fluorescence (WD-XRF) using a PW-2404 spectrometer (Panalytical). Details of the analytical protocols are provided by Formenti et al. (2008). The concentration of water-soluble ions were determined by Ion chromatography (IC) with a Metrohm IC 850 device equipped with an injection loop of 100 µL. For anionic species, IC has been

ACPD
15, 21607–21669, 2015

equipped with Metrosep A supp 16 (250/4.0 mm) column associated with a metrosepA supp 16 guard pre-column heated at 65 °C. For simultaneous separation of inorganic and short-chain organic anions, elution has been realized with eluant composed at 20 % by ultrapure water and at 80 % by a solution 7.5 mM Na_2CO_3 and 0.75 mM NaOH. The elution flow rate was 0.8 mL min^{-1}. For cationic species, IC has been equipped with a Metrosep C4 (250/4.0 mm) column associated to a metrosep C4 guard column heated at 30 °C. Elution has been realized with an eluant composed with 0.7 mM of dipicolinic acid and 1.7 mM of nitric acid. The elution flow rate was 1 mL min^{-1}.

The mass concentration of refractory black carbon particles (rBC) was measured using a single particle soot photometer (SP2, DMT). The SP2 uses a continuous intracavity Nd:YAG laser at the wavelength of 1064 nm to heat rBC-containing particles to their vaporization point. Single particle rBC mass was derived from the peak intensity of the thermal radiation emitted by the incandescent rBC detected by the SP2. This method allows the quantification with 100 % efficiency of rBC mass in single particles with mass equivalent diameters between 80–500 nm (Moteki and Kondo, 2010). The total rBC mass loading was reported as the sum of all the detected single particle rBC masses. Prior to the measurement field campaign, the SP2 was calibrated using fullerene soot particles, which have been shown to give similar SP2 response as ambient rBC (Moteki and Kondo, 2010; Baumgardner et al., 2012; Laborde et al., 2012).

2.2.3 Aerosol scattering and extinction coefficients

The particle scattering coefficient (σ_{scat}) was measured at three wavelengths (450, 550 and 700 nm) with an integrating nephelometer (TSI, model 3563), which integrates light scattered by particles at scattering angle between the incident and scattered radiation between 7 and 170°. The instrument operated at a volumetric flow rate of 30 L min^{-1} and the data were acquired at 1 s time resolution. The instrument was calibrated with free-particle air and high-purity CO_2 prior to and after the campaign. Measured values were corrected for the angular truncature error in the nephelometer measurements at angles smaller than 7° and greater than 170° as described in Sect. 2.3.2.

ACPD
15, 21607–21669, 2015

The particle extinction coefficient (σ_{ext}) was measured with a Cavity Attenuated Phase Shift particle light extinction monitor (CAPS-PMex, Aerodyne Research) operated at the wavelength of 530 nm. The instrument relies on measuring the average time spent by the light within the sample cell. The sampling volumetric flowrate was 0.85 L min^{-1} and data were processed with a time resolution of 1 s.

2.3 Aerosol data analysis

Figure 2 depicts the iterative procedure used to retrieve the aerosol size distribution and optical parameters relevant to this paper. We focused our attention on aerosol parameters used in climate models for calculating the direct and semi-direct aerosol radiative effects:

- The complex refractive index $\widetilde{n}$ defined as $n_r - in_i$, where n_r and n_i are the real and imaginary part representing the particle scattering and absorption properties, respectively.
- The single scattering albedo ω_0 (unitless) representing the balance between the scattering and the absorbing properties and defined as:

$$\omega_0(\lambda) = \frac{\sigma_{scat}(\lambda)}{\sigma_{ext}(\lambda)} \quad (1)$$

where σ_{scat} is the aerosol scattering coefficient (expressed in Mm^{-1} = 10^{-6} m^{-1}), σ_{ext} the aerosol extinction coefficient (M m^{-1}) and λ the wavelength (nm).

- The asymmetry parameter g (unitless) describing the angular distribution of the scattered radiation and defined as:

$$g(\lambda) = \frac{1}{2}\int_0^{\pi} \cos(\theta)\sin(\theta)P(\theta,\lambda)\,d\theta \quad (2)$$

where $P(\theta,\lambda)$ is the scattering phase function and θ is the scattering angle.

ACPD
15, 21607–21669, 2015

– The mass extinction efficiency k_{ext} ($m^2\,g^{-1}$) representing the total light extinction per unit mass concentration of aerosol and calculated as:

$$k_{ext}(\lambda) = \frac{\sigma_{ext}(\lambda)}{C_m} \quad (3)$$

where C_m is the aerosol mass concentration ($\mu g\,m^{-3}$).

2.3.1 Assessment of aerosol size distribution

The particle size distribution was derived from the SMPS, UHSAS, GRIMM and FSSP-300. For size distributions measured by SMPS, the electrical mobility D_m and the geometric particle diameters D_g are related by the dynamic shape factor χ (DeCarlo et al., 2004):

$$D_g = \frac{D_m}{\chi} \quad (4)$$

The dynamic shape factor χ depends on the shape of the particles (Hinds, 1999). Dust particles are predominantly non-spherical (Chou et al., 2008). In this study, we have decided to neglect the non-sphericity of mineral dust to maintain retrieval conditions similar to those of previous literature studies on dust in source region. Henceforth, χ was set to unity.

Optical sizing instruments (i.e. UHSAS, GRIMM, FSSP-300) measure the amount of light scattered by a single particle and convert this into a geometric particle size. This conversion depends on the complex refractive index of the aerosol, as well as on the optical geometry and the laser wavelength of the instrument. The correction procedure used the Mie scattering theory for homogeneous spheres with known complex refractive index (Bohren and Huffman, 1983). As discussed by Reid et al. (2003), the conversion of scattered light into particle size can lead to ambiguity in the sizing of the coarse mode diameters. If the light intensity response of the optical sizing instruments is non-unique it can lead to oversizing of larger particles. This happens mostly

ACPD
15, 21607–21669, 2015

for forward scattering probes, such as the FSSP-300, as demonstrated in Fig. S1 in the Supplement showing a flattening in the scattering cross section curves integrated over the FSSP-300 scattering angle range (3–15°) between 2 and 10 µm diameter. For the GRIMM 1.129 scattering angles (30–150°), the scattering cross section is unique with size, except between 1.5–2 µm where an inflection point can be seen. Given the response curves in Fig. S1, data between 2–10 and 1.5–2 µm diameter from the FSSP-300 and the GRIMM, respectively, were not considered in this paper.

Figure 3 presents an example of size distributions measured in a dust plume by the different instruments. As will be discussed below, the value of $\widetilde{n} = 1.53–0.004i$ at 530 nm was the most appropriate to restitute both scattering and extinction coefficient and therefore we present results using this value in Fig. 3. Overall, the comparison between different instruments shows good consistency, giving credence to the measurements and the choice of refractive index and dynamic shape factor.

The resulting number and volume size distributions were parameterized by fitting four log-normal distributions, as:

$$\frac{\mathrm{d}N}{\mathrm{d}\log D_\mathrm{p}} = \sum_{i=1}^{4} \frac{N_{\mathrm{tot},i}}{\sqrt{2\pi}\cdot\log\sigma_i} \exp\left[-\frac{(\log D_\mathrm{p} - \log D_{\mathrm{p,g},i})^2}{2(\log\sigma_i)^2}\right] \quad (5)$$

$$\frac{\mathrm{d}V}{\mathrm{d}\log D_\mathrm{p}} = \sum_{i=1}^{4} \frac{N_{\mathrm{tot,\,i}}\cdot\frac{\pi}{6}\cdot D_\mathrm{p}^3}{\sqrt{2\pi}\cdot\log\sigma_i} \exp\left[-\frac{(\log D_\mathrm{p} - \log D_{\mathrm{p,g},i})^2}{2(\log\sigma_i)^2}\right] \quad (6)$$

each mode i being characterized by characterized by the integrated number concentration $N_{\mathrm{tot},i}$, the geometric median diameter $D_{\mathrm{p,g},i}$ and the geometric standard deviation σ_i (i.e. Fig. 3).

To provide a synthetic representation of the particle number size distributions, the effective particle D_eff was calculated as:

$$D_\mathrm{eff} = \frac{\int D_\mathrm{p}^3 \frac{\mathrm{d}N}{\mathrm{d}D_\mathrm{g}}\mathrm{d}D_\mathrm{p}}{\int D_\mathrm{p}^2 \frac{\mathrm{d}N}{\mathrm{d}D_\mathrm{p}}\mathrm{d}D_\mathrm{p}} \quad (7)$$

ACPD
15, 21607–21669, 2015

D_{eff} has been estimated separately on the fine and coarse fractions in the size ranges 0.053–1 µm (refered as $D_{eff,f}$ thereafter) and 1–32 µm (refered as $D_{eff,c}$), respectively.

2.3.2 Assessment of aerosol optical properties

An iterative procedure was used to derive $\widetilde{n}$, ω_0, g and k_{ext} at 530 nm and correct σ_{scat} for the angular truncature error (i.e. Fig. 2). The parametrized size distributions were used as input for the Mie scattering calculations (Bohren and Huffman, 1983), which were done by varying stepwise the real part of the complex refractive index n_r from 1.33 to 1.60 and the imaginary part of the complex refractive index n_i from 0.000 to 0.020. $\widetilde{n}$ was assumed to be constant with particle size and have thus to be regarded as an effective value for the entire particle population. σ_{scat} was adjusted to the CAPS operation wavelength of 530 nm by using the following equation:

$$\text{Å}(\lambda_1,\lambda_2) = -\frac{\ln(\sigma_{scat}(\lambda_1)/\sigma_{scat}(\lambda_2))}{\ln(\lambda_1/\lambda_2)} \quad (8)$$

where Å represents the spectral dependence of the scattering coefficient and λ_1 and λ_2 are the wavelength interval. The scattering Angstrom exponent Å is often used as a qualitative indicator of aerosol particle size or fine mode fraction (Seinfeld and Pandis, 1998). Typically, it is lower than ~ 0.5 for aerosols dominated by coarse particles, such as mineral dust or sea salt, but it is higher than 1 for fine particles, such as pollution particles or biomass burning. The calculated values of σ_{scat} (530 nm) and σ_{ext} (530 nm) were compared to that measured by the nephelometer and the CAPS, and values having the closest agreement within the measurement error bars were chosen as the best estimate.

The in-aircraft aerosol instruments sampled through isokinetic and isoaxial aerosol inlets. Particle loss can however occur both as a result of the inlet aspiration efficiency and the transport losses in the pipework between the inlet and the instruments. The

ACPD
15, 21607–21669, 2015

cut-off diameter, at which the passing efficiency of the inlet equals 50 %, happened at around 12 µm for the AVIRAD inlet and 5 µm for the Community Aerosol Inlet in equivalent optical diameter. Mie scattering calculations were performed using either the size distribution measured behind the aircraft inlets or the full size distribution to assess the impact of the size-selective aircraft inlets on optical parameters. The absolute errors associated with n_r, n_i, ω_0, g and k_{ext} due to the passing efficiencies of the inlets were in the range covered by the measurements uncertainties of both optical parameters and size distributions, which were estimated to be 0.02, 0.002, 0.04, 0.05 and 0.08, respectively.

2.4 Ancillary products

Weather Research and Forecasting (WRF; Skamarock et al., 2008) simulations were performed to investigate the meteorological conditions and the turbulence within the dust layers. The WRF model is operational at the Department of Physics of the University of Genoa, Italy, in a three-domain configuration. In particular, the simulations on the parent domain, covering the entire Mediterranean basin with a horizontal grid spacing of 10 km, have been considered for the present paper. Initial and boundary conditions were generated from the operational global model GFS (Environmental Modeling Center, 2003) outputs (0.5° × 0.5° resolution). More details about the modelling chain and the model setup are given in Bove et al. (2014), Cassola et al. (2015), and Mentaschi et al. (2015).

As a complement, synoptic conditions and sea level pressure composite anomalies over the Mediterranean basin during the campaign were analyzed using reanalysis data sets, such as the NCEP/NCAR Reanalysis (Kalnay et al., 1996) and the NCEP Climate Forecast System (CFS) reanalysis (Saha et al., 2010).

Source regions and atmospheric transport times of the dust plumes were determined through the combination of satellite products and backward trajectories analysis. The potential source regions active during the observational period were identified using the images from the Spinning Enhanced Visible and Infrared Imager (SEVIRI) onboard

ACPD
15, 21607–21669, 2015

the Meteosat Second Generation (MSG) satellite. The NOAA HYbrid Single-Particle Lagrangian Integrated Trajectory Model (HYSPLIT, http://www.arl.noaa.gov/HYSPLIT.php) using the Global Data Assimilation System (GDAS) meteorological input was used to calculate whether an air mass sampled by the aircraft could have originated from one of the identified active dust sources. Backward trajectories were initialized using the time and the location when the aircraft intercepted the air mass and were extended for up to 5 days prior the measurement. Backward trajectory calculations were performed at the beginning, the middle and at the end of each SLR to check the origin and transport pathway of the air masses through the measurements. We then operationally define the dust age as the time elapsed since the calculated air mass trajectory leave the ground where an active source was detected and the time of sampling by the aircraft.

3 Results

3.1 Identification of the dust source region and transport pathway

During the ADRIMED campaign, the synoptic situation was characterized by a "dipolar" sea level pressure anomaly pattern, with positive anomalies in the western Mediterranean and negative ones in the eastern part of the basin, as illustrated in Fig. 4 (left panel). While this situation induced stronger and more frequent than normal northwesterly winds over the Sardinia and Sicily channels, the average conditions at upper atmospheric levels during the campaign were closer to climatological ones (Fig. 4, right panel). Relatively frequent dust episodes could be observed as it is typical for the season (Moulin et al., 1998).

The synoptic conditions during each of the 9 flights described in Fig. 1 and Table 1 are summarized in Figs. S2 and S3 in the Supplement, where sea level pressure and 500 hPa geopotential height are shown. A low-pressure system can be found over the Atlantic on 16 June, moving towards the Iberian Peninsula, while a subtropical ridge

ACPD
15, 21607–21669, 2015

extends from North Africa to Central Mediterranean. This situation induced a strong south-southwesterly flow, firstly towards Southern Iberia and western Mediterranean (16–17 June), then extending eastwards and reaching Corsica on the subsequent days, favouring dust transport from the Saharan region. This is quite evident from Fig. S4, showing 700 hPa wind and relative humidity maps from the WRF model. Figure 1 shows the likely sources regions for dust sampled during the flights, identified from HYSPLIT simulation and MSG-SEVIRI satellite products. Mineral dust were most likely uplifted from southern Morocco and Southern Algeria and were sampled during flights F29, F30, F31 and F32 after 3.5–4.5 days of transport.

On 19–20 June the remnants of the aforementioned low are still visible as an upper level trough over the western Mediterranean (Fig. S4), triggering meridional transport at higher levels from North Algeria/Tunisia region towards the Sardinia and Sicily Channels. This is confirmed by backward trajectory and satellite product analyses showing that the dust sampled during the flight F33–34 travelled 1 to 5 days from North Algeria/Tunisia before their sampling (not shown). On 28 June during flight F38, an upper level low is found over the Alps and Central Europe, inducing a westerly flow from Tunisia where mineral dust were most likely uptlifted towards Sicily at 700 hPa (Fig. S5), while the surface high pressure over East Atlantic and Iberia is associated to northwesterly winds at lower levels throughout most of Central Mediterranean. Finally, the situation during the last flight F42 (3 July) was characterized by a modest depression over Iberia, while the Azores anticyclone extended towards the Mediterranean. As a consequence, upper level winds were mainly southwesterly over North Africa, veering to westerly or northwesterly over the Sardinia and Sicily Channel, thus contributing to dust transport in the area. We estimate that mineral dust originating from South Morroco and Tunisia was transported for 3.5 days before sampling.

The identification of the dust source regions was confirmed by the measurements of the elemental composition. Overall, Si/Al ranged between 2.4–2.7 and Fe/Ca between 0.3–0.7 in the samples collected during ADRIMED. This is consistent with values previously reported for mineral dust originating from Algeria, Tunisia and Morocco

ACPD
15, 21607–21669, 2015

(Scheuvens et al., 2013; Formenti et al., 2014). The identified emission areas also correspond to known source regions such as the Grand Erg occidental at the border between Algeria and Morocco, the Mekkeranne in Algeria and the Chott El Jerïd in Tunisia (Ginoux et al., 2012).

3.2 Vertical distribution of mineral dust

Figure 5 shows the vertical profiles of the aerosol scattering coefficient σ_{scat} at λ = 450, 550 and 700 nm, the total particle number concentration in the submicron (N_{fine}; 5 nm < D_p < 1 µm) and the supermicron (N_{coarse}; D_p > 1 µm) size ranges, and the vertical distribution of the scattering Angstrom exponent Å calculated between 450 and 770 nm. The top height of the boundary layer (Z_b) and the wind shear level (Z_s) are also indicated in Fig. 5 by a solid and a dashed line, respectively. All the vertical profiles were characterized by a weak and positive gradient of the potential temperature, characteristic of a stratified atmosphere (Fig. S6). The top height of the boundary layer was identified as the height at which the temperature profile showed the highest discontinuity and the water vapor mixing ratio decreased the most rapidly. The shear level was determined from the sudden increase in wind speed and change in wind direction (Fig. S6).

Mineral dust was observed above the boundary layer in layers extending from 1 km to more than 6 km a.s.l. (Fig. 5). The presence of mineral dust within the boundary layer was not attested neither by chemical analyses nor with the back-trajectories analyses, which revealed that in the 5 days prior sampling, low-level air masses originated from the European continent or recirculated within Mediterranean basin. The transport of mineral dust in the free troposphere up to 9 km in altitude is a common observation in the Mediterranean region, as previously reported by lidar measurements (Dulac and Chazette, 2003; Mona et al., 2006; Di Iorio et al., 2009; Gómez-Amo et al., 2011). Such high altitudes may be linked to the strong vertical convective processes over the dust source regions, which lift dust particles at high atmospheric levels (Flamant et al., 2007; Papayannis et al., 2008; Cuesta et al., 2009).

ACPD
15, 21607–21669, 2015

The dust vertical structures showed an important variability. Complex and stratified structures were observed depending on the position of Z_b and Z_s. During the campaign, the wind shear level was equal to or higher than the top of the boundary layer.

When Z_s and Z_b coincided (F30, F31, F32, F38), the dust vertical structure was characterized by a single and rather homogeneous layer. It is noteworthy that apparently similar thermo-dynamical situations displayed a different spectral dependence of the scattering coefficient, as for example is the case above the boundary layer for flights F32 (Å ∼ 0.3) and F38 (Å ∼ 0.9), pointing out differences in the particle type. The values of Å observed during the flight F38 were higher than the values of ∼ 0.5 reported for Saharan dust in source region (McConnell et al., 2008a; Muller et al., 2011), but lower than values of Å > 1 reported for air masses dominated by pollution aerosols in the western Mediterranean basin (Di Biagio et al., 2015). It is reasonable to suppose that the profile F38 reflects a situation where desert dust was mixed with pollution particles. This is confirmed by the five-day backward trajectories (Fig. 6a), which indicates air parcel coming from Europe and traveling at least three days above the Mediterranean Sea within the boundary level before its uplift over Tunisia.

When Z_s was higher than Z_b (F33, F34, F35), mineral dust was found in two distinct layers at intermediate (between 1–3 km a.s.l.) and elevated altitude (above 3 km a.s.l.). The five-day backward trajectories suggest that these dust layers originated from different dust source regions (Fig. 1 and Table 1). An example is given by the flight F35 (Fig. 6b) for which the elevated dust layer originated from central Algeria and was carried by northern flow to Lampedusa in 3.5 days, whereas the dust layer at intermediate altitude was transported from the southeastern Morocco-southwestern Algeria border region by a westerly flow within 3 days. Similar structure with multilayering of the Saharan dust corresponding to air masses from different dust source regions was previously observed by lidar measurements in the Mediterranean region (Hamonou et al., 1999; Guerrero-Rascado et al., 2008).

Regardless of the thermo-dynamical structure of the atmosphere, the aerosol vertical profiles revealed a clear vertical variability of the contribution of fine mode particles in

ACPD
15, 21607–21669, 2015

the dust layers. The values of N_{fine} and Å were generally below 1000 # cm^{-3} and 0.5, respectively, in elevated dust layers. In contrast, N_{fine} and Å were up to 4000 # cm^{-3} and 2.2, respectively, in the intermediate dust altitude (Fig. 5). These observations suggest that either the intermediate dust plumes carried more fine particles during transport at intermediate altitude or dust particles in the fine mode exhibited a vertical gradient.

3.3 Size distribution of the dust plumes

Particle number size distributions classified as a function of altitude are shown in Fig. 7. Table 3 presents the average characteristics of the parameterized four-modal number size distributions.

In the fine mode, the size distributions showed three modes around 80, 120 and 320 nm (Fig. 7a). For particles smaller than 300 nm, the shapes of the size distributions in the dust layer and in the boundary layer were quite similar. As particles in this size range mostly reflect anthropogenic influences from near or distant sources (Birmili et al., 2010), this indicates that the pollution plumes from the surface were exported above the boundary layer and mixed with the dust layers. The particle size distributions in the elevated dust layers followed a similar pattern as in the intermediate dust layers but number concentrations 2 times smaller were observed for the modes at 80 and 120 nm, suggesting that the concentration of pollution particles varied with the altitude. For particles between 300 nm and 1 µm, the particle size distributions were reasonably constant for dust layers at various altitudes. Kaaden et al. (2008) found dust particles as small as 300 nm diameter in Morroco, which was also confirmed by Kandler et al. (2009). The decrease of N_{fine} with altitude (i.e. Fig. 5) was therefore most likely due to the larger concentration of sub-300 nm pollution particles transported in the intermediate dust plumes. The fact that an identical median diameter $D_{p,g}$ was used to parameterize the number size distributions in the fine mode at intermediate and elevated layers (Table 3) and the prevalence of a sub-300 nm particles in the intermediate

ACPD
15, 21607–21669, 2015

dust layer (Fig. 7a) might also reflect that the mixing between the pollution and the dust plumes was mostly external in the fine mode.

In the coarse mode, a modal diameter of the number size distribution between 1.3 and 2.0 µm was observed indiscriminately to dust altitude. This indicates that the dust layers transported over the Mediterranean basin were well-mixed vertically in terms of coarse particle population, as previously observed by Weinzierl et al. (2011) for mineral dust after short-range transport over the eastern Atlantic Ocean. Conversely, the number concentration of large dust particles decreased with increasing altitude for freshly uplifted Saharan dust (Weinzierl et al., 2009; Ryder et al., 2013a). There are some evidences suggesting that the well-vertical mixing of the dust plumes occurs during the first day following the dust uplifted (Ryder et al., 2013b). Turbulent fluxes within the dust layer might be responsible for the vertical distribution of the dust aerosols becoming more homogeneous in terms of coarse mode particles as the dust ages (Rosenberg et al., 2014). Particles in the coarse mode showed a large flight-to-flight variability with number concentrations varying by more than one order of magnitude. This is quite evident in Fig. 7b showing the conversion of number size distributions into volume size distributions. This variation in concentration might reflect the wide range of dust event encountered during the campaign in terms of source regions, time of transport and meteorological conditions.

The comparison of volume size distributions obtained during ADRIMED with those measured during other airborne campaigns close to dust source regions (AMMA, FENNEC and SAMUM-1) showed a good overlapping in the peak of the coarse mode (Fig. 7c). Effective diameters of the coarse mode $D_{\mathrm{eff,c}}$ ranged from 3.8 to 14.2 µm during ADRIMED, which is in the range of magnitude of the mean values of 3.8, 8.8 and 7.4 µm obtained during AMMA, FENNEC and SAMUM-1, respectively (Formenti et al., 2011b; Ryder et al., 2013a; Weinzierl et al., 2011). Contrastingly, fewer particles larger than 10 µm were uncounted after short-range transport over the eastern Atlantic Ocean in the Cape-Verde region during SAMUM-2 with respect to the other campaigns. $D_{\mathrm{eff,c}}$ around 3.2 µm was found in the dust layers during SAMUM-2 (Weinzierl et al., 2011).

ACPD
15, 21607–21669, 2015

3.4 Optical properties of the dust plumes

Figure 8a and b shows the vertical distribution of the real and imaginary parts of the refractive index $\tilde{n}$. Within the dust plumes, $\tilde{n}$ ranged from 1.50 to 1.55 for the real part and remained below 0.005 for the imaginary part. Since $\tilde{n}$ is related to the aerosol chemical composition (Liu and Daum, 2008), it is expected to be influenced by the mixing rate of the dust plume with pollution particles. We thus plotted the values of $\tilde{n}$ as a function of the Angstrom exponent Å. Besides not displaying significant variation with the altitude, the values of $\tilde{n}$ did not show any dependence on Å. The results obtained during ADRIMED have been compared with data in the literature for Saharan dust in or near-sources in Fig. 8. For both the real and imaginary parts, our estimates of $\tilde{n}$ fall within the range of variability (1.51–1.57 and 0.0001–0.0046 for the real and the imaginary parts, respectively) documented in source regions (Schladitz et al., 2009; Formenti et al., 2011a; Ryder et al., 2013b). This variability was attributed to the variability of the mineralogical composition of dust originating from diverse source regions (Kandler et al., 2009; Petzold et al., 2009). Our data do not show any clear dependence of $\tilde{n}$ on dust source region either (not shown), which is consistent with the limited regional variability of the dust optical properties found 1–2 days after emissions in Africa by Formenti et al. (2014) from aircraft measurements. This is probably a consequence of the mixing of dust from various active sources occurring with each other during transport shortly after emission. A number of uncertainties in our identification of dust source region is associated with the employed methodology. The trajectory error associated with calculation of back trajectories from HYSPLIT reaches 15–30 % of the travel distance (Draxler and Rolph, 2013). Another potential source of uncertainty is the difficulty to discriminate the satellite aerosol signals from the surface reflectance using MSG-SEVIRI observations, especially over bright surfaces (Kutuzov et al., 2013). Moreover, even if the origin of the air masses was checked at the beginning, the middle and at the end of each straight-levelled runs, larger number of sources could potentially contribute to the aircraft samples because of aircraft's movements during sampling.

ACPD
15, 21607–21669, 2015

The vertical distribution of intensive optical properties relevant to radiative transfer (i.e. single scattering albedo ω_0, asymmetry parameter g and extinction mass efficiency k_{ext}) are shown in Fig. 8c–e and Table 4. Estimates of ω_0, g and k_{ext} fall within the range 0.90–1.00, 0.6–0.8 and 0.3–0.7 $m^2 g^{-1}$, respectively. Overall, there is not clear dependence on the altitude. Only slightly low values of g (from ~ 0.7 to ~ 0.8) and k_{ext} (from ~ 0.3 to ~ 0.7 $m^2 g^{-1}$) were observed for some dust layers below 3 km a.s.l. As $\tilde{n}$ was found to be constant with the altitude (i.e. Fig. 8a and b), these variations in g and k_{ext} were probably due to the variability in particles size distributions, which is consistent with the larger fraction of fine particles found in these dust layers (i.e. Fig. 7a). Values of ω_0, g and k_{ext} remained, however, within the range of values reported in source regions by Schladitz et al. (2009), Formenti et al. (2011a) and Ryder et al. (2013b). Despite the fact that dust plumes carried pollution particles during their long-range transport in the Mediterranean region, the dust optical properties appeared to be unaffected by this mixing.

In the Mediterranean region, previous estimates of ω_0 for dust particles were obtained from remote-sensing techniques. Mallet et al. (2013) reported from multi-year ground-based AERONET observations a column-averaged ω_0 of 0.92–0.95 between 440–880 nm for various sites over the Mediterranean under the influence of dust aerosols. Using a similar approach, Di Biagio et al. (2009) reported lower column-averaged ω_0 values during dust transport events when boundary-layer air masses are transported from central Europe, probably rich in absorbing particles from urban-industrial European areas. Values as low as 0.88 at 530 nm were also determined by Sicard et al. (2012) during a case study of a dust plume transported over Barcelona and accompanied by a biomass-burning outbreak. Recently, Valenzuela et al. (2014) presented eight months of dust optical properties over the Alborán Island from Sun photometer measurements for dust plumes originating from northwestern Africa and passing over several urban-industrial areas along the coast of Morocco and from eastern Africa and traveling over the Mediterranean Sea. No significant changes in column-averaged ω_0 were reported for the different air masses, which indicates that the influ-

ACPD
15, 21607–21669, 2015

ence of anthropogenic fine particles originating from the urban-industrial areas in the north of Africa during desert dust outbreaks was negligible. Overall, these contrasting results highlight the major role of the transport conditions (height, air mass encountered) of the dust plumes rather than the dust source region in governing the dust layer optical properties in the Mediterranean.

4 Discussion

4.1 On the role of transport conditions in the mixing of pollution particles with mineral dust

In this section, we investigate the transport conditions of the dust layers expected to influence the mixing of mineral dust with pollution particles. As previously mentioned, the highest concentrations of pollution particles were detected in the intermediate dust layers. We further investigate this result by examining the variations of $D_{\mathrm{eff,f}}$ and $D_{\mathrm{eff,c}}$ with the altitude of the dust plumes. We assume that changes in $D_{\mathrm{eff,f}}$ reflected different fractions of externally mixed pollution particles smaller than 300 nm in the dust plumes, as discussed in Sect. 3.3. In Fig. 9a and a sharp transition in the proportion of fine particles can be seen in $D_{\mathrm{eff,f}}$ at 3 km a.s.l. with greater proportion of pollution particles found in the lower 3 km of the atmosphere. The observation of pollution particles at altitudes up to 3 km during ADRIMED is comparable with the average height of pollution layers observed in the western Mediterranean basin (Meloni et al., 2003; Mallet et al., 2005; Junkermann et al., 2009; Di Biagio et al., 2015). Hence, the vertical extent of pollution particles might explain the fact that the intermediate dust plumes were more affected by fine particles than the elevated dust layer. The coarse mode of the dust plume is also expected to be impacted by the presence of pollution particles. In case of an internal mixing between pollution particles and mineral dust, the mean particles size should increase. During ADRIMED, $D_{\mathrm{eff,c}}$ of the dust plume did not show any systematic dependence on altitude (Fig. 9b). This finding must however be interpreted with some

ACPD
15, 21607–21669, 2015

caution since $D_{\mathrm{eff,\,c}}$ was affected by the large uncertainties in FSSP-300 and GRIMM sizing (i.e. Sect. 2.2.1.) that might hide the detection of small aggregates on dust.

The mixing extent of pollution particles in dust layers is also expected to depend on the transport time of the plumes. Figure 10 shows $D_{\mathrm{eff,f}}$ against the estimated age of the dust air mass and divided according to the height of transport of the dust plumes. From these measurements, we do not find significant trend in the dust mixing rate with transport time in both elevated and intermediate layers. This result is not surprising for the elevated dust layers since we found that the interaction of dust plumes with pollution particles was limited when they were transported above 3 km a.s.l. For dust plumes below 3 km a.s.l., their transport time was at least 3 days before sampling during ADRIMED. Afterwards the dust spent time over pollution regions appeared to have no more effect on the mixing extent of pollution particles. The constant $D_{\mathrm{eff,f}}$ values observed within the intermediate dust plumes and the boundary layer (Fig. 9a) suggests also that the vertical transport and mixing of pollution particles with dust plumes were already completed at the time of sampling. Note that the intermediate dust layers reached the Mediterranean coasts affected by urban/industrial emissions after having undergone around 2 days of transport. Hence, the pollution mixing rate appears to be a relatively rapid process more likely driven by the height of transport of the dust layers.

4.2 Contribution of pollution particles to the absorption properties of the dust plumes

We evaluated the effect of the contribution of pollution particles to the absorption properties of the dust layers by calculating ω_0 from the mass concentration of the main anthropogenic compounds. Table 5 shows the mass concentration of major elements, ionic species and rBC measured in the dust plumes. The dust mass concentration estimated from the measured Al using the mean Al mass fraction in the crustal composition of 7.09 % (Guieux et al., 2002) is also shown. In all samples, silicates were the most abundant type of dust particles, as expected from previous chemical analysis of dust in North Africa (Scheuvens et al., 2013; Formenti et al., 2014). The presence of pollution

ACPD
15, 21607–21669, 2015

particles within the dust plumes is confirmed by the detection of SO_4^{2-} and rBC as well as typical anthropogenic trace elements such as V, Pb and Zn.

SO_4^{2-} reached concentrations typical of the Mediterranean region in summertime (Ripoll et al., 2015) with the largest concentration of 2.5 µg m^{-3} found over Corsica during the flight F34. The positive correlation between the concentration of SO_4^2 and N_{fine} indicates the presence of externally mixed sulfate-containing particles in the fine mode particles, such as ammonium sulfate particles. SO_4^2/NH_4^+ ratios being higher than unity, the presence of SO_4^{2-} in the dust layers can also either be due to nucleation of sulfuric acid in polluted plumes, or to sulphate formation at the surface of preexistent particles by uptake of gaseous sulfur dioxide or by coagulation of sulphate particles (Ullerstam et al., 2002; Korhonen et al., 2003; Sullivan et al., 2009).

Concentrations of rBC ranged from 0.04 to 0.13 µg m^{-3}. Although these values are much lower than concentrations measured in areas of high industrial or traffic density (Liu et al., 2014; Mantas et al., 2014), they are in agreement with concentrations found in continental and background area of the western Mediterranean (Ripoll et al., 2015). Except in the case of large forest fires, rBC concentrations are generally low on average in summertime due to the absence of the major sources of emission, such as domestic wood burning (Tsyro et al., 2007).

Calculations of ω_0 from the aerosol chemical composition were performed assuming that dust was externally mixed with rBC and sulfate. Indeed, prevalence of an external mixing between dust particles and rBC has been observed from long-term measurements in the western Mediterranean basin (Ripoll et al., 2015). Moreover, coating of sulfate on mineral dust has been shown to have no significant effect on dust optical properties (Bauer et al., 2007). We used mean mass absorption and extinction efficiencies (i.e. the total light absorption or extinction per unit mass of aerosol, referred as k_{abs} and k_{ext}) of 0.02 and 0.64 $m^2\,g^{-1}$ for dust (Hess et al., 1998), 7.5 and 9.4 $m^2\,g^{-1}$ for rBC (Bond and Bergstrom, 2006) and 0 and 5.0 $m^2\,g^{-1}$ for sulfate (Charlson et al., 1992). As shown in Table 5, ω_0 obtained from this calculation ranged from 0.93–0.97,

ACPD
15, 21607–21669, 2015

which falls within the range of values obtained from measurements (0.92–0.99 ± 0.04). For comparison, we estimate that ω_0 for pure mineral dust was 0.97. This simple approach confirms the small influence of pollution particles on the optical properties of the dust plumes over the Mediterranean region.

4.3 Retention of coarse mode particles in the dust plumes

Figure 11 shows $D_{\mathrm{eff,c}}$ against the estimated age of the dust air mass. Observations from aircraft during previous campaigns are shown for comparison. The $D_{\mathrm{eff,c}}$ values did not change with time, suggesting that the dust layers transported over the Mediterranean region tend to conserve their coarse mode with time. Values obtained during ADRIMED are consistent with those obtained near dust source regions within 1.5 days after emission (Formenti et al., 2011b; Weinzierl et al., 2011; Ryder et al., 2013b), but, for a comparable transport time, higher than after long-range transport over the Atlantic ocean (Maring et al., 2003; Weinzierl et al., 2011).

The loss of large dust particles after transport as observed over the Atlantic Ocean is most likely associated to the removal processes occurring as the dust travels downwind (Mahowald et al., 2014). As smaller particles fall downward much slower than larger particles, coarse particles are expected to be more prevalent close to the sources regions. To date only few studies have focused on understanding the evolution of dust size distribution, especially during transport over the Atlantic Ocean (Maring et al., 2003; Reid et al., 2003; Kalashnikova and Kahn, 2008). These measurements pointed out large differences between the observed and modeled evolution of dust size, with a lifetime of coarse particles longer than expected from deposition theories. This suggests that other processes counterbalanced the loss of large particles by dry deposition along transport. These processes seem to be particularly important in the Mediterranean region, since the proportional volume of coarse particles in the size distribution did not vary substantially even after 5 days of transport.

The persistence of coarse particles over the Mediterranean basin during transport could be explained by the presence of temperature inversions in the middle tropo-

ACPD
15, 21607–21669, 2015

sphere keeping the dust layers confined due to the stable stratification. This was revealed by most of the aircraft temperature profiles (Fig. S6). Furthermore, the WRF model simulations of the vertical velocity and vertical cross-section indicate the existence of updraft/downdraft due to the thermal turbulence within the dust layers circulating over the Mediterranean basin in summertime, due to elevated temperatures within the dust layers and large insolation. An example for flight F33 in the Corsica region is shown in Fig. 12, where the vertical velocity showed updrafts and downdrafts up to 0.5 Pa s^{-1}, corresponding to about 5 cm s^{-1}. This value is at least one order of magnitude greater than the gravitational settling velocity (0.25 cm s^{-1}) expected for particles of 8 µm diameter, value indicated by Maring et al. (2003) as the threshold above which sensible changes in dust size distribution during atmospheric transport across the Atlantic could be observed. The occurence of turbulent updraft and downdraft motion could therefore result in an enhancement of the particle lifetime in the atmosphere over the Mediterranean basin.

5 Conclusions

We presented the first in situ aircraft measurements of the size distribution and optical properties of Saharan dust transported over the western Mediterranean basin within the framework of the ADRIMED airborne campaign in June–July 2013. Dust particles originating from Algeria, Tunisia and Morocco were sampled in the western Mediterranean basin after 1–5 days of transport.

Measurements of aerosol vertical profiles revealed that dust particles were transported inside well-defined layers above the boundary layer (> 1 km a.s.l.) dominated by pollution and marine particles. The dust vertical structure was extremely variable and characterized either by a single layer or a more complex and stratified structure. Backward trajectories indicated that the multilayering of the Saharan dust corresponded to air masses originating from different dust source regions. Abundance of sub-300 nm particles in the Saharan dust layers suggested a strong mixing of dust with pollution

ACPD
15, 21607–21669, 2015

particles. The height of transport of the dust layers appeared to be the main factor affecting the mixing extent of pollution particles with mineral dust. Mineral dust carried higher concentration of pollution particles at intermediate altitude (1–3 km a.s.l.) than at elevated altitude (> 3 km a.s.l.), resulting in scattering Angstrom exponent up to 2.2 within the intermediate layer. This coincides with the typical height of pollution layers (∼ 3 km a.s.l.) observed in the western Mediterranean basin.

The optical properties of the dust layers were not significantly affected by this mixing with respect to values reported for native dust. Mineral dust aerosols were found to be moderately absorbing with values of ω_0 between 0.90 and 1.00 at 530 nm. Concurrent optical calculations from the aerosol chemical composition revealed that the contribution of pollution particles to absorption properties of the dust plumes was negligible. This was most likely due to the low contribution of rBC (∼ 2 % in mass) in regards to the fraction of dust (∼ 84 %) and sulfate (∼ 14 %) in the dust plumes. The concentrations of anthropogenic particles being typical of those observed in the Mediterranean region in summertime, these results demonstrate that outside severe episode of pollution or biomass burning, mineral dust dominate the optical properties of the dust plumes in the Mediterranean even if source of pollution particles are present.

An important question for the dust direct, semi-direct and indirect radiative effects is how long the coarse mode of dust particles is conserved during transport. We showed that the coarse mode was conserved even after 5 days of transport in the Mediterranean, which contrasts with the gravitational depletion of large dust particles observed during the transport of dust over the Atlantic Ocean. The global importance of this result is however still linked to whether these observations are ubiquitous or occur only for specific dust transport events. Dust events differing in terms of source region, time and height for transport were reported in this study. For all these case studies, the coarse mode of dust particles was conserved during transport, which might reflect the representativeness of the situation mostly occuring in summertime in the western Mediterranean bassin.

ACPD
15, 21607–21669, 2015

Most climate models simulate currently the dry deposition as a positive relationship of the particles size, leading in an underestimation of the fraction of coarse particles being transported long distances (Mahowald et al., 2014). Given the scarcity of field studies investigating the evolution of the dust size distribution during transport, our results point out key processes controlling the retention of large dust aerosols. In particular, WRF model simulations highlighted a strong turbulence within the dust layer with vertical velocity at least one order of magnitude greater than the particle gravitational settling velocity. Particles could therefore remain trapped in the atmosphere by this strong turbulence. Further studies involving a deep analysis of aircraft measurements of turbulence parameters both in the Mediterranean and in other geographical areas such as the Atlantic region are required in order to quantitatively characterize this process and improve the representativeness of the temporal evolution of dust size distribution in climate models useful for radiative impact or marine biogeochemical applications.

The dataset obtained during the ADRIMED airborne campaign can also be used for constraining satellite retrievals that make assumptions on dust properties in order to derive water vapor profiles, surface temperatures and greenhouse gases concentrations. The results presented here suggest that the size and optical properties of the dust plumes could be assimilated to those of native dust in satellite retrievals in the western Mediterranean. Moreover, this important dataset provides opportunities for evaluating satellite aerosol products (size, absorption properties, vertical profiles) over the Mediterranean through comparison with our in-situ airborne measurements.

In terms of significance for direct and semi-direct radiative effects, the presence of moderately absorbing particles within the dust layers can induce important modifications in the tropospheric heating and surface cooling by perturbing the incoming and outgoing radiations. Evidence for retention of coarse mode particles in the dust layers indicates also that mineral dust may still be a significant source of cloud condensation nuclei and ice nuclei despite having undergone long-range transport. Hence, mineral dust may have potentially important implications for the regional climate and the rain-

ACPD
15, 21607–21669, 2015

fall patterns in the west Mediterranean that should be quantitatively adressed in future modelling studies.

The Supplement related to this article is available online at doi:10.5194/acpd-15-21607-2015-supplement.

Acknowledgements. This research work has been supported by the French National Research Agency (ANR) through the ADRIMED program (contract ANR-11-BS56-0006). This work is part of the ChArMEx project supported by CNRS-INSU, ADEME, Météo-France and CEA in the framework of the multidisciplinary program MISTRALS (Mediterranean Integrated Studies aT Regional And Local Scales; http://mistrals-home.org/). The aircraft deployment was also supported by CNES. We thank the instrument scientists, pilots and ground crew of SAFIRE for facilitating the instrument integration and conducting flying operations. We acknowledge Pierre Nabat and the ENM students, especially Damien Serça, Jonathan Guth and Valentin Seigner for their meteorological forecasts during the campaign. We thank the NOAA Air Resources Laboratory (ARL) for the provision of the HYSPLIT transport and dispersion model used in this study.

References

Andreae, M. O. and Merlet, P.: Emission of trace gases and aerosols from biomass burning, Global Biogeochem. Cy., 15, 955–966, doi:10.1029/2000GB001382, 2001.

Andreae, M. O. and Rosenfeld, D.: Aerosol-cloud-precipitation interactions, Part 1, the nature and sources of cloud-active aerosols, Earth.-Sci. Rev., 89, 13–41, 2008.

Ansmann, A., Baars, H., Tesche, M., Müller, D., Althausen, D., Engelmann, R., Pauliquevis, T., and Artaxo, P.: Dust and smoke transport from Africa to South America: lidar profiling over Cape Verde and the Amazon rainforest, Geophys. Res. Lett., 36, L11802, doi:10.1029/2009GL037923, 2009.

Basart, S., Pérez, C., Cuevas, E., Baldasano, J. M., and Gobbi, G. P.: Aerosol characterization in Northern Africa, Northeastern Atlantic, Mediterranean Basin and Middle East from direct-

ACPD
15, 21607–21669, 2015

sun AERONET observations, Atmos. Chem. Phys., 9, 8265–8282, doi:10.5194/acp-9-8265-2009, 2009.
Bauer, S. E., Mishchenko, M. I., Lacis, A. A., Zhang, S., Perlwitz, J., and Metzger, S. M.: Do sulphate and nitrate coatings on mineral dust have important effects on radiative properties and climate modeling?, J. Geophys. Res.-Atmos., 112, D06307, doi:10.1029/2005JD006977, 2007.
Baumgardner, D., Dye, J. E., Gandrud, B. W., and Knollenberg, R. G.: Interpretation of measurements made by forward scattering probe (FSSP-300) during the airborne arctic stratospheric expedition, J. Geophys. Res.-Atmos., 97, 8035–8046, 1992.
Baumgardner, D., Popovicheva, O., Allan, J., Bernardoni, V., Cao, J., Cavalli, F., Cozic, J., Diapouli, E., Eleftheriadis, K., Genberg, P. J., Gonzalez, C., Gysel, M., John, A., Kirchstetter, T. W., Kuhlbusch, T. A. J., Laborde, M., Lack, D., Müller, T., Niessner, R., Petzold, A., Piazzalunga, A., Putaud, J. P., Schwarz, J., Sheridan, P., Subramanian, R., Swietlicki, E., Valli, G., Vecchi, R., and Viana, M.: Soot reference materials for instrument calibration and intercomparisons: a workshop summary with recommendations, Atmos. Meas. Tech., 5, 1869–1887, doi:10.5194/amt-5-1869-2012, 2012.
Bègue, N., Tulet, P., Chaboureau, J. P., Roberts, G., Gomes, L., and Mallet, M.: Long-range transport of Saharan dust over northwestern Europe during EUCAARI 2008 campaign: evolution of dust optical properties by scavenging, J. Geophys. Res.-Atmos, 117, D17201, doi:10.1029/2012jd017611, 2012.
Birmili, W., Heinke, K., Pitz, M., Matschullat, J., Wiedensohler, A., Cyrys, J., Wichmann, H.-E., and Peters, A.: Particle number size distributions in urban air before and after volatilisation, Atmos. Chem. Phys., 10, 4643–4660, doi:10.5194/acp-10-4643-2010, 2010.
Bohren, C. F. and Huffman, D. R.: Absorption and scattering of light by small particles, Wiley, New York, 1983.
Bove, M. C., Brotto, P., Cassola, F., Cuccia, E., Massabò, D., Mazzino, A., Piazzalunga, A., and Prati, P.: An integrated $PM_{2.5}$ source apportionment study: positive matrix factorization vs. the chemical transport model CAMx, Atmos. Environ., 94, 274–286, 2014.
Cai, Y., Montague, D. C., Mooiweer-Bryan, W., and Deshler, T.: Performance characteristics of the ultra high sensitivity aerosol spectrometer for particles between 55 and 800 nm: laboratory and field studies, J. Aerosol Sci., 39, 759–769, doi:10.1016/j.jaerosci.2008.04.007, 2008.

ACPD
15, 21607–21669, 2015

Cassola, F., Ferrari, F., and Mazzino, A.: Numerical simulations of Mediterranean heavy precipitation events with the WRF model: a verification exercise using dierent approaches, Atmos. Res., 164–165, 210–225, doi:10.1016/j.atmosres.2015.05.010, 2015.

Charlson, R. J., Schwartz, S. E., Hales, J. M., Cess, R. D., Coakley, J. A., Hansen, J. E., and Hofmann, D. J.: Climate forcing by anthropogenic aerosols, Science, 255, 423–430, doi:10.1126/science.255.5043.423, 1992.

Choobari, O. A., Zawar-Reza, P., and Sturman, A.: The global distribution of mineral dust and its impacts on the climate system: a review, Atmos. Res., 138, 152–165, doi:10.1016/j.atmosres.2013.11.007, 2014.

Chou, C., Formenti, P., Maille, M., Ausset, P., Helas, G., Harrison, M., and Osborne, S.: Size distribution, shape, and composition of mineral dust aerosols collected during the African monsoon multidisciplinary analysis special observation period 0: dust and biomass-burning experiment field campaign in Niger, January 2006, J. Geophys. Res.-Atmos., 113, D00C10, doi:10.1029/2008JD009897, 2008.

Clarke, A. D., Shinozuka, Y., Kapustin, V. N., Howell, S., Huebert, B., Doherty, S., Anderson, T., Covert, D., Anderson, J., Hua, X., Moore, K. G., McNaughton, C., Carmichael, G., and Weber, R.: Size distributions and mixtures of dust and black carbon aerosol in Asian outflow: physiochemistry and optical properties, J. Geophys. Res.-Atmos., 109, D15S09, doi:10.1029/2003JD004378, 2004.

Collaud Coen, M., Weingartner, E., Schaub, D., Hueglin, C., Corrigan, C., Henning, S., Schwikowski, M., and Baltensperger, U.: Saharan dust events at the Jungfraujoch: detection by wavelength dependence of the single scattering albedo and first climatology analysis, Atmos. Chem. Phys., 4, 2465–2480, doi:10.5194/acp-4-2465-2004, 2004.

Crumeyrolle, S., Gomes, L., Tulet, P., Matsuki, A., Schwarzenboeck, A., and Crahan, K.: Increase of the aerosol hygroscopicity by cloud processing in a mesoscale convective system: a case study from the AMMA campaign, Atmos. Chem. Phys., 8, 6907–6924, doi:10.5194/acp-8-6907-2008, 2008.

Cuesta, J., Marsham, J. H., Parker, D. J., and Flamant, C.: Dynamical mechanisms controlling the vertical redistribution of dust and the thermodynamic structure of the West Saharan atmospheric boundary layer during summer, Atmos. Sci. Lett., 10, 34–42, doi:10.1002/asl.207, 2009.

d'Almeida, G. A.: A model for Saharan dust transport, J. Clim. Appl. Meteorol., 25, 903–916, doi:10.1175/1520-0450(1986)025<0903:AMFSDT>2.0.CO;2, 1986.

ACPD
15, 21607–21669, 2015

DeCarlo, P., Slowik, J., Worsnop, D., Davidovits, P., and Jimenez, J.: Particle morphology and density characterization by combined mobility and aerodynamic diameter measurements, Part 1: Theory, Aerosol Sci. Tech., 38, 1185–1205, 2004.
de Meij, A. and Lelieveld, J.: Evaluating aerosol optical properties observed by ground-based and satellite remote sensing over the Mediterranean and the Middle East in 2006, Atmos. Res., 99, 415–433, doi:10.1016/j.atmosres.2010.11.005, 2011.
Di Biagio, C., di Sarra, A., Meloni, D., Monteleone, F., Piacentino, S., and Sferlazzo, D.: Measurements of Mediterranean aerosol radiative forcing and influence of the single scattering albedo, J. Geophys. Res.-Atmos., 114, D06211, doi:10.1029/2008JD011037, 2009.
Di Biagio, C., Doppler, L., Gaimoz, C., Grand, N., Ancellet, G., Raut, J.-C., Beekmann, M., Borbon, A., Sartelet, K., Attié, J.-L., Ravetta, F., and Formenti, P.: Continental pollution in the Western Mediterranean Basin: vertical profiles of aerosol and trace gases measured over the sea during TRAQA 2012 and SAFMED 2013, Atmos. Chem. Phys. Discuss., 15, 8283–8328, doi:10.5194/acpd-15-8283-2015, 2015.
Di Iorio, T., di Sarra, A., Sferlazzo, D. M., Cacciani, M., Meloni, D., Monteleone, F., Fuà, D., and Fiocco, G.: Seasonal evolution of the tropospheric aerosol vertical profile in the central Mediterranean and role of desert dust, J. Geophys. Res.-Atmos., 114, D02201, doi:10.1029/2008JD010593, 2009.
Draxler, R. R. and Rolph, G. D.: HYSPLIT (HYbrid Single-Particle Lagrangian Integrated Trajectory) Model access via NOAA ARL READY Website (http://ready.arl.noaa.gov/HYSPLI~T.php), NOAA Air Resources Laboratory, Silver Spring, MD, 2015.
Doherty, O. M., Riemer, N., and Hameed, S.: Saharan mineral dust transport into the Caribbean: observed atmospheric controls and trends, J. Geophys. Res.-Atmos., 113, doi:10.1029/2007jd009171, 2008.
Dulac, F. and Chazette, P.: Airborne study of a multi-layer aerosol structure in the eastern Mediterranean observed with the airborne polarized lidar ALEX during a STAAARTE campaign (7 June 1997), Atmos. Chem. Phys., 3, 1817–1831, doi:10.5194/acp-3-1817-2003, 2003.
Engelstaedter, S., Tegen, I., and Washington, R.: North African dust emissions and transport, Earth.-Sci. Rev., 79, 73–100, doi:10.1016/j.earscirev.2006.06.004, 2006.
Environmental Modeling Center: The GFS Atmospheric Model, NCEP Office Note 442, National Oceanic and Atmospheric Administration, Global Climate and Weather Modeling Branch,

ACPD
15, 21607–21669, 2015

EMC, Camp Springs: Maryland, 14 pp., available at: http://www.emc.ncep.noaa.gov/gmb/moorthi/gam.html (last access: 10 August 2015), 2003.

Fan, X.-B., Okada, K., Niimura, N., Kai, K., Arao, K., Shi, G.-Y., Qin, Y., and Mitsuta, Y.: Mineral particles collected in china and japan during the same Asian dust-storm event, Atmos. Environ., 30, 347–351, doi:10.1016/1352-2310(95)00271-Y, 1996.

Flamant, C., Chaboureau, J. P., Parker, D. J., Taylor, C. M., Cammas, J. P., Bock, O., Timouk, F., and Pelon, J.: Airborne observations of the impact of a convective system on the planetary boundary layer thermodynamics and aerosol distribution in the inter-tropical discontinuity region of the West African Monsoon, Q. J. Roy. Meteor. Soc., 133, 1175–1189, doi:10.1002/qj.97, 2007.

Formenti, P., Andreae, M. O., Lange, L., Roberts, G., Cafmeyer, J., Rajta, I., Maenhaut, W., Holben, B. N., Artaxo, P., and Lelieveld, J.: Saharan dust in Brazil and Suriname during the large-scale biosphere–atmosphere experiment in Amazonia (LBA) – cooperative LBA regional experiment (CLAIRE) in March 1998, J. Geophys. Res.-Atmos., 106, 14919–14934, doi:10.1029/2000JD900827, 2001.

Formenti, P., Elbert, W., Maenhaut, W., Haywood, J., and Andreae, M. O.: Chemical composition of mineral dust aerosol during the Saharan dust experiment (SHADE) airborne campaign in the Cape Verde region, September 2000, J. Geophys. Res.-Atmos., 108, 8576, doi:10.1029/2002JD002648, 2003.

Formenti, P., Rajot, J. L., Desboeufs, K., Caquineau, S., Chevaillier, S., Nava, S., Gaudichet, A., Journet, E., Triquet, S., Alfaro, S., Chiari, M., Haywood, J., Coe, H., and Highwood, E.: Regional variability of the composition of mineral dust from western Africa: results from the AMMA SOP0/DABEX and DODO field campaigns, J. Geophys. Res.-Atmos., 113, D00C13, doi:10.1029/2008JD009903, 2008.

Formenti, P., Rajot, J. L., Desboeufs, K., Saïd, F., Grand, N., Chevaillier, S., and Schmechtig, C.: Airborne observations of mineral dust over western Africa in the summer Monsoon season: spatial and vertical variability of physico-chemical and optical properties, Atmos. Chem. Phys., 11, 6387–6410, doi:10.5194/acp-11-6387-2011, 2011a.

Formenti, P., Schütz, L., Balkanski, Y., Desboeufs, K., Ebert, M., Kandler, K., Petzold, A., Scheuvens, D., Weinbruch, S., and Zhang, D.: Recent progress in understanding physical and chemical properties of African and Asian mineral dust, Atmos. Chem. Phys., 11, 8231–8256, doi:10.5194/acp-11-8231-2011, 2011b.

ACPD
15, 21607–21669, 2015

Formenti, P., Caquineau, S., Desboeufs, K., Klaver, A., Chevaillier, S., Journet, E., and Rajot, J. L.: Mapping the physico-chemical properties of mineral dust in western Africa: mineralogical composition, Atmos. Chem. Phys., 14, 10663–10686, doi:10.5194/acp-14-10663-2014, 2014.

Garrett, T. J., Russell, L. M., Ramaswamy, V., Maria, S. F., and Huebert, B. J.: Microphysical and radiative evolution of aerosol plumes over the tropical North Atlantic Ocean, J. Geophys. Res.-Atmos., 108, 4022, doi:10.1029/2002JD002228, 2003.

Gkikas, A., Houssos, E. E., Hatzianastassiou, N., Papadimas, C. D., and Bartzokas, A.: Synoptic conditions favouring the occurrence of aerosol episodes over the broader Mediterranean basin, Q. J. Roy. Meteor. Soc., 138, 932–949, doi:10.1002/qj.978, 2012.

Ginoux, P., Prospero, J. M., Gill, T. E., Hsu, N. C., and Zhao, M.: Global-scale attribution of anthropogenic and natural dust sources and their emission rates based on MODIS Deep Blue aerosol products, Rev. Geophys., 50, RG3005, doi:10.1029/2012RG000388, 2012.

Gómez-Amo, J. L., Pinti, V., Di Iorio, T., di Sarra, A., Meloni, D., Becagli, S., Bellantone, V., Cacciani, M., Fuà, D., and Perrone, M. R.: The June 2007 Saharan dust event in the central Mediterranean: observations and radiative effects in marine, urban, and sub-urban environments, Atmos. Environ., 45, 5385–5393, doi:10.1016/j.atmosenv.2011.06.045, 2011.

Goudie, A. S. and Middleton, N. J.: Saharan dust storms: nature and consequences, Earth.-Sci. Rev., 56, 179–204, doi:10.1016/S0012-8252(01)00067-8, 2001.

Guerrero-Rascado, J. L., Ruiz, B., and Alados-Arboledas, L.: Multi-spectral Lidar characterization of the vertical structure of Saharan dust aerosol over southern Spain, Atmos. Environ., 42, 2668–2681, doi:10.1016/j.atmosenv.2007.12.062, 2008.

Guieu, C., Loÿe-Pilot, M. D., Ridame, C., and Thomas, C.: Chemical characterization of the Saharan dust end-member: some biogeochemical implications for the western Mediterranean Sea, J. Geophys. Res.-Atmos., 107, ACH5.1–ACH5.11, doi:10.1029/2001JD000582, 2002.

Hamonou, E., Chazette, P., Balis, D., Dulac, F., Schneider, X., Galani, E., Ancellet, G., and Papayannis, A.: Characterization of the vertical structure of Saharan dust export to the Mediterranean basin, J. Geophys. Res.-Atmos., 104, 22257–22270, doi:10.1029/1999JD900257, 1999.

Haywood, J. M., Johnson, B. T., Osborne, S. R., Baran, A. J., Brooks, M., Milton, S. F., Mulcahy, J., Walters, D., Allan, R. P., Klaver, A., Formenti, P., Brindley, H. E., Christopher, S., and Gupta, P.: Motivation, rationale and key results from the GERBILS Saharan dust measurement campaign, Q. J. Roy. Meteor. Soc., 137, 1106–1116, doi:10.1002/qj.797, 2011.

ACPD
15, 21607–21669, 2015

Heintzenberg, J.: The SAMUM-1 experiment over Southern Morocco: overview and introduction, Tellus B, 61, 2–11, doi:10.1111/j.1600-0889.2008.00403.x, 2009.
Hess, M., Koepke, P., and Schult, I.: Optical properties of aerosols and clouds: the software package OPAC, B. Am. Meteorol. Soc., 79, 831–844, doi:10.1175/1520-0477(1998)079<0831:OPOAAC>2.0.CO;2, 1998.
Hinds, W. C.: Aerosol Technology: Properties, Behavior, and Measurement of Airborne Particles, 2nd Edn., Wiley, New York, 1999.
Huneeus, N., Chevallier, F., and Boucher, O.: Estimating aerosol emissions by assimilating observed aerosol optical depth in a global aerosol model, Atmos. Chem. Phys., 12, 4585–4606, doi:10.5194/acp-12-4585-2012, 2012.
IPCC: Fifth assessment report – the physical science basis, available at: http://www.ipcc.ch, last access: 7 October 2013.
Jing Su, Jianping Huang, Qiang Fu, Minnis, P., Jinming Ge, and Jianrong Bi: Estimation of Asian dust aerosol effect on cloud radiation forcing using Fu-Liou radiative model and CERES measurements, Atmos. Chem. Phys., 8, 2763–2771, doi:10.5194/acp-8-2763-2008, 2008.
Junkermann, W.: On the distribution of formaldehyde in the western Po-Valley, Italy, during FORMAT 2002/2003, Atmos. Chem. Phys., 9, 9187–9196, doi:10.5194/acp-9-9187-2009, 2009.
Kaaden, N., Massling, A., Schladitz, A., Muller, T., Kandler, K., Schutz, L., Weinzierl, B., Petzold, A., Tesche, M., Leinert, S., Deutscher, C., Ebert, M., Weinbruch, S., and Wiedensohler, A.: State of mixing, shape factor, number size distribution, and hygroscopic growth of the Saharan anthropogenic and mineral dust aerosol at Tinfou, Morocco, Tellus B, 61, 51–63, doi:10.1111/j.1600-0889.2008.00388.x, 2009.
Kalashnikova, O. V. and Kahn, R. A.: Mineral dust plume evolution over the Atlantic from MISR and MODIS aerosol retrievals, J. Geophys. Res.-Atmos., 113, D24204, doi:10.1029/2008JD010083, 2008.
Kalnay, E., Kanamitsu, M., Kistler, R., Collins, W., Deaven, D., Gandin, L., Iredell, M., Saha, S., White, G., Woollen, J., Zhu, Y., Leetmaa, A., Reynolds, R., Chelliah, M., Ebisuzaki, W., Higgins, W., Janowiak, J., Mo, K. C., Ropelewski, C., Wang, J., Jenne, R., and Joseph, D.: The NCEP/NCAR 40-Year Reanalysis Project, B. Am. Meteorol. Soc., 77, 437–471, doi:10.1175/1520-0477(1996)077<0437:TNYRP>2.0.CO;2, 1996.
Kandler, K., Schütz, L., Deutscher, C., Ebert, M., Hofmann, H., Jäckel, S., Jaenicke, R., Knippertz, P., Lieke, K., Massling, A., Petzold, A., Schladitz, A., Weinzierl, B., Wiedensohler, A.,

ACPD
15, 21607–21669, 2015

Zorn, S., and Weinbruch, S.: Size distribution, mass concentration, chemical and mineralogical composition and derived optical parameters of the boundary layer aerosol at Tinfou, Morocco, during SAMUM 2006, Tellus B, 61, 32–50, doi:10.1111/j.1600-0889.2008.00385.x, 2009.

Kanitz, T., Engelmann, R., Heinold, B., Baars, H., Skupin, A., and Ansmann, A.: Tracking the Saharan Air Layer with shipborne lidar across the tropical Atlantic, Geophys. Res. Lett., 41, 1044–1050, doi:10.1002/2013GL058780, 2014.

Koçak, M., Theodosi, C., Zarmpas, P., Séguret, M. J. M., Herut, B., Kallos, G., Mihalopoulos, N., Kubilay, N., and Nimmo, M.: Influence of mineral dust transport on the chemical composition and physical properties of the Eastern Mediterranean aerosol, Atmos. Environ., 57, 266–277, doi:10.1016/j.atmosenv.2012.04.006, 2012.

Koehler, K. A., Kreidenweis, S. M., DeMott, P. J., Petters, M. D., Prenni, A. J., and Carrico, C. M.: Hygroscopicity and cloud droplet activation of mineral dust aerosol, Geophys. Res. Lett., 36, L08805, doi:10.1029/2009GL037348, 2009.

Korhonen, H., Napari, I., Timmreck, C., Vehkamäki, H., Pirjola, L., Lehtinen, K. E. J., Lauri, A., and Kulmala, M.: Heterogeneous nucleation as a potential sulphate-coating mechanism of atmospheric mineral dust particles and implications of coated dust on new particle formation, J. Geophys. Res.-Atmos., 108, 4546, doi:10.1029/2003JD003553, 2003.

Koren, I., Joseph, J. H., and Israelevich, P.: Detection of dust plumes and their sources in northeastern Libya, Can. J. Remote Sens., 29, 792–796, doi:10.5589/m03-036, 2003.

Kutuzov, S., Shahgedanova, M., Mikhalenko, V., Ginot, P., Lavrentiev, I., and Kemp, S.: High-resolution provenance of desert dust deposited on Mt. Elbrus, Caucasus in 2009–2012 using snow pit and firn core records, The Cryosphere, 7, 1481–1498, doi:10.5194/tc-7-1481-2013, 2013.

Laborde, M., Mertes, P., Zieger, P., Dommen, J., Baltensperger, U., and Gysel, M.: Sensitivity of the Single Particle Soot Photometer to different black carbon types, Atmos. Meas. Tech., 5, 1031–1043, doi:10.5194/amt-5-1031-2012, 2012.

Lack, D. A. and Cappa, C. D.: Impact of brown and clear carbon on light absorption enhancement, single scatter albedo and absorption wavelength dependence of black carbon, Atmos. Chem. Phys., 10, 4207–4220, doi:10.5194/acp-10-4207-2010, 2010.

Levin, Z., Ganor, E., and Gladstein, V.: The effects of desert particles coated with sulfate on rain formation in the Eastern Mediterranean, J. Appl. Meteorol., 35, 1511–1523, doi:10.1175/1520-0450(1996)035<1511:TEODPC>2.0.CO;2, 1996.

ACPD
15, 21607–21669, 2015

Levin, Z., Teller, A., Ganor, E., and Yin, Y.: On the interactions of mineral dust, sea-salt particles, and clouds: a measurement and modeling study from the Mediterranean Israeli Dust Experiment campaign, J. Geophys. Res.-Atmos., 110, D20202, doi:10.1029/2005JD005810, 2005.

Liu, Y. G. and Daum, P. H.: Relationship of refractive index to mass density and self-consistency of mixing rules for multicomponent mixtures like ambient aerosols, J. Aerosol Sci., 39, 974–986, doi:10.1016/j.jaerosci.2008.06.006, 2008.

Liu, D., Allan, J. D., Young, D. E., Coe, H., Beddows, D., Fleming, Z. L., Flynn, M. J., Gallagher, M. W., Harrison, R. M., Lee, J., Prevot, A. S. H., Taylor, J. W., Yin, J., Williams, P. I., and Zotter, P.: Size distribution, mixing state and source apportionment of black carbon aerosol in London during wintertime, Atmos. Chem. Phys., 14, 10061–10084, doi:10.5194/acp-14-10061-2014, 2014.

Ma, Q. X., Liu, Y. C., Liu, C., and He, H.: Heterogeneous reaction of acetic acid on MgO, alpha-Al_2O_3, and $CaCO_3$ and the effect on the hygroscopic behaviour of these particles, Phys. Chem. Chem. Phys., 14, 8403–8409, doi:10.1039/c2cp40510e, 2012.

Mahowald, N., Albani, S., Kok, J. F., Engelstaeder, S., Scanza, R., Ward, D. S., and Flanner, M. G.: The size distribution of desert dust aerosols and its impact on the Earth system, Aeolian Research, 15, 53–71, doi:10.1016/j.aeolia.2013.09.002, 2014.

Mallet, M., Van Dingenen, R., Roger, J. C., Despiau, S., and Cachier, H.: In situ airborne measurements of aerosol optical properties during photochemical pollution events, J. Geophys. Res.-Atmos., 110, doi:10.1029/2004jd005139, 2005.

Mallet, M., Dubovik, O., Nabat, P., Dulac, F., Kahn, R., Sciare, J., Paronis, D., and Léon, J. F.: Absorption properties of Mediterranean aerosols obtained from multi-year ground-based remote sensing observations, Atmos. Chem. Phys., 13, 9195–9210, doi:10.5194/acp-13-9195-2013, 2013.

Mallet, M., Dulac, F., Formenti, P., Nabat, P., Sciare, J., Roberts, G., Pelon, J., Ancellet, G., Tanré, D., Parol, F., di Sarra, A., Alados, L., Arndt, J., Auriol, F., Blarel, L., Bourrianne, T., Brogniez, G., Chazette, P., Chevaillier, S., Claeys, M., D'Anna, B., Denjean, C., Derimian, Y., Desboeufs, K., Di Iorio, T., Doussin, J.-F., Durand, P., Féron, A., Freney, E., Gaimoz, C., Goloub, P., Gómez-Amo, J. L., Granados-Muñoz, M. J., Grand, N., Hamonou, E., Jankowiak, I., Jeannot, M., Léon, J.-F., Maillé, M., Mailler, S., Meloni, D., Menut, L., Momboisse, G., Nicolas, J., Podvin, J., Pont, V., Rea, G., Renard, J.-B., Roblou, L., Schepanski, K., Schwarzenboeck, A., Sellegri, K., Sicard, M., Solmon, F., Somot, S., Torres, B., Totems, J.,

ACPD
15, 21607–21669, 2015

Triquet, S., Verdier, N., Verwaerde, C., Wenger, J., and Zapf, P.: Overview of the Chemistry-Aerosol Mediterranean Experiment/Aerosol Direct Radiative Forcing on the Mediterranean Climate (ChArMEx/ADRIMED) summer 2013 campaign, Atmos. Chem. Phys. Discuss., 15, 19615–19727, doi:10.5194/acpd-15-19615-2015, 2015.

Mantas, E., Remoundaki, E., Halari, I., Kassomenos, P., Theodosi, C., Hatzikioseyian, A., and Mihalopoulos, N.: Mass closure and source apportionment of $PM_{2.5}$ by Positive Matrix Factorization analysis in urban Mediterranean environment, Atmos. Environ., 94, 154–163, doi:10.1016/j.atmosenv.2014.05.002, 2014.

Marconi, M., Sferlazzo, D. M., Becagli, S., Bommarito, C., Calzolai, G., Chiari, M., di Sarra, A., Ghedini, C., Gómez-Amo, J. L., Lucarelli, F., Meloni, D., Monteleone, F., Nava, S., Pace, G., Piacentino, S., Rugi, F., Severi, M., Traversi, R., and Udisti, R.: Saharan dust aerosol over the central Mediterranean Sea: PM_{10} chemical composition and concentration versus optical columnar measurements, Atmos. Chem. Phys., 14, 2039–2054, doi:10.5194/acp-14-2039-2014, 2014.

Maring, H., Savoie, D. L., Izaguirre, M. A., Custals, L., and Reid, J. S.: Mineral dust aerosol size distribution change during atmospheric transport, J. Geophys. Res.-Atmos., 108, doi:10.1029/2002jd002536, 2003.

McConnell, C. L., Highwood, E. J., Coe, H., Formenti, P., Anderson, B., Osborne, S., Nava, S., Desboeufs, K., Chen, G., and Harrison, M. A. J.: Seasonal variations of the physical and optical characteristics of Saharan dust: results from the dust outflow and deposition to the ocean (DODO) experiment, J. Geophys. Res.-Atmos., 113 D14S05, doi:10.1029/2007jd009606, 2008.

Meloni, D., di Sarra, A., DeLuisi, J., Di Iorio, T., Fiocco, G., Junkermann, W., and Pace, G.: Tropospheric aerosols in the Mediterranean: 2. radiative effects through model simulations and measurements, J. Geophys. Res.-Atmos., 108, 4317, doi:10.1029/2002JD002807, 2003.

Meloni, D., di Sarra, A., Pace, G., and Monteleone, F.: Aerosol optical properties at Lampedusa (Central Mediterranean). 2. Determination of single scattering albedo at two wavelengths for different aerosol types, Atmos. Chem. Phys., 6, 715–727, doi:10.5194/acp-6-715-2006, 2006.

Mentaschi, L., Besio, G., Cassola, F., and Mazzino, A.: Performance evaluation of WavewatchIII in the Mediterranean Sea, Ocean Model., 90, 82–94, doi:10.1016/j.ocemod.2015.04.003, 2015.

ACPD
15, 21607–21669, 2015

Mona, L., Amodeo, A., Pandolfi, M., and Pappalardo, G.: Saharan dust intrusions in the Mediterranean area: three years of Raman lidar measurements, J. Geophys. Res.-Atmos., 111, D16203, doi:10.1029/2005JD006569, 2006.
Moteki, N. and Kondo, Y.: Dependence of laser-induced incandescence on physical properties of black carbon aerosols: measurements and theoretical interpretation, Aerosol Sci. Tech., 44, 663–675, doi:10.1080/02786826.2010.484450, 2010.
Moulin, C., Lambert, C. E., Dulac, F., and Dayan, U.: Control of atmospheric export of dust from North Africa by the North Atlantic oscillation, Nature, 387, 691–694, 1997.
Moulin, C., Lambert, C. E., Dayan, U., Masson, V., Ramonet, M., Bousquet, P., Legrand, M., Balkanski, Y. J., Guelle, W., Marticorena, B., Bergametti, G., and Dulac, F.: Satellite climatology of African dust transport in the Mediterranean atmosphere, J. Geophys. Res.-Atmos., 103, 13137–13144, doi:10.1029/98JD00171, 1998.
Muller, T., Schladitz, A., Kandler, K., and Wiedensohler, A.: Spectral particle absorption coefficients, single scattering albedos and imaginary parts of refractive indices from ground based in situ measurements at Cape Verde Island during SAMUM-2, Tellus B, 63, 573–588, doi:10.1111/j.1600-0889.2011.00572.x, 2011.
Osborne, S. R., Johnson, B. T., Haywood, J. M., Baran, A. J., Harrison, M. A. J., and McConnell, C. L.: Physical and optical properties of mineral dust aerosol during the dust and biomass-burning experiment, J. Geophys. Res.-Atmos., 113, D00C03, doi:10.1029/2007jd009551, 2008.
Otto, S., Bierwirth, E., Weinzierl, B., Kandler, K., Esselborn, M., Tesche, M., Schladitz, A., Wendisch, M., and Trautmann, T.: Solar radiative effects of a Saharan dust plume observed during SAMUM assuming spheroidal model particles, Tellus B, 61, 270–296, doi:10.1111/j.1600-0889.2008.00389.x, 2009.
Papayannis, A., Amiridis, V., Mona, L., Tsaknakis, G., Balis, D., Bosenberg, J., Chaikovski, A., De Tomasi, F., Grigorov, I., Mattis, I., Mitev, V., Muller, D., Nickovic, S., Perez, C., Pietruczuk, A., Pisani, G., Ravetta, F., Rizi, V., Sicard, M., Trickl, T., Wiegner, M., Gerding, M., Mamouri, R. E., D'Amico, G., and Pappalardo, G.: Systematic lidar observations of Saharan dust over Europe in the frame of EARLINET (2000–2002), J. Geophys. Res.-Atmos., 113, D10204, doi:10.1029/2007jd009028, 2008.
Perrone, M. R. and Bergamo, A.: Direct radiative forcing during Sahara dust intrusions at a site in the Central Mediterranean: anthropogenic particle contribution, Atmos. Res., 101, 783–798, doi:10.1016/j.atmosres.2011.05.011, 2011.

ACPD
15, 21607–21669, 2015

Perry, K. D., Cahill, T. A., Eldred, R. A., Dutcher, D. D., and Gill, T. E.: Long-range transport of North African dust to the eastern United States, J. Geophys. Res.-Atmos., 102, 11225–11238, doi:10.1029/97JD00260, 1997.

Petzold, A., Rasp, K., Weinzierl, B., Esselborn, M., Hamburger, T., Dörnbrack, A., Kandler, K., Schütz, L., Knippertz, P., Fiebig, M., and Virkkula, A. K. I.: Saharan dust absorption and refractive index from aircraft-based observations during SAMUM 2006, Tellus B, 61, 118–130, doi:10.1111/j.1600-0889.2008.00383.x, 2009.

Pey, J., Querol, X., Alastuey, A., Forastiere, F., and Stafoggia, M.: African dust outbreaks over the Mediterranean Basin during 2001–2011: PM_{10} concentrations, phenomenology and trends, and its relation with synoptic and mesoscale meteorology, Atmos. Chem. Phys., 13, 1395–1410, doi:10.5194/acp-13-1395-2013, 2013.

Prospero, J. M., Ginoux, P., Torres, O., Nicholson, S. E., and Gill, T. E.: Environmental characterization of global sources of atmospheric soil dust identified with the nimbus 7 total ozone mapping spectrometer (TOMS) absorbing aerosol product, Rev. Geophys., 40, 1002, doi:10.1029/2000RG000095, 2002.

Querol, X., Alastuey, A., Pey, J., Cusack, M., Pérez, N., Mihalopoulos, N., Theodosi, C., Gerasopoulos, E., Kubilay, N., and Koçak, M.: Variability in regional background aerosols within the Mediterranean, Atmos. Chem. Phys., 9, 4575–4591, doi:10.5194/acp-9-4575-2009, 2009.

Reid, J. S., Kinney, J. E., Westphal, D. L., Holben, B. N., Welton, E. J., Tsay, S.-C., Eleuterio, D. P., Campbell, J. R., Christopher, S. A., Colarco, P. R., Jonsson, H. H., Livingston, J. M., Maring, H. B., Meier, M. L., Pilewskie, P., Prospero, J. M., Reid, E. A., Remer, L. A., Russell, P. B., Savoie, D. L., Smirnov, A., and Tanré, D.: Analysis of measurements of Saharan dust by airborne and ground-based remote sensing methods during the Puerto Rico dust experiment (PRIDE), J. Geophys. Res.-Atmos., 108, 8586, doi:10.1029/2002JD002493, 2003.

Ripoll, A., Minguillón, M. C., Pey, J., Pérez, N., Querol, X., and Alastuey, A.: Joint analysis of continental and regional background environments in the western Mediterranean: PM_1 and PM_{10} concentrations and composition, Atmos. Chem. Phys., 15, 1129–1145, doi:10.5194/acp-15-1129-2015, 2015.

Rosenberg, P. D., Parker, D. J., Ryder, C. L., Marsham, J. H., Garcia-Carreras, L., Dorsey, J. R., Brooks, I. M., Dean, A. R., Crosier, J., McQuaid, J. B., and Washington, R.: Quantifying

ACPD
15, 21607–21669, 2015

particle size and turbulent scale dependence of dust flux in the Sahara using aircraft measurements, J. Geophys. Res.-Atmos., 119, 7577–7598, doi:10.1002/2013JD021255, 2014.
Rosenfeld, D., Rudich, Y., and Lahav, R.: Desert dust suppressing precipitation: a possible desertification feedback loop, P. Natl. Ac. Sci., 98, 5975–5980, doi:10.1073/pnas.101122798, 2001.
Ryder, C. L., Highwood, E. J., Lai, T. M., Sodemann, H., and Marsham, J. H.: Impact of atmospheric transport on the evolution of microphysical and optical properties of Saharan dust, Geophys. Res. Lett., 40, 2433–2438, doi:10.1002/grl.50482, 2013a.
Ryder, C. L., Highwood, E. J., Rosenberg, P. D., Trembath, J., Brooke, J. K., Bart, M., Dean, A., Crosier, J., Dorsey, J., Brindley, H., Banks, J., Marsham, J. H., McQuaid, J. B., Sodemann, H., and Washington, R.: Optical properties of Saharan dust aerosol and contribution from the coarse mode as measured during the Fennec 2011 aircraft campaign, Atmos. Chem. Phys., 13, 303–325, doi:10.5194/acp-13-303-2013, 2013b.
Saha, A., Mallet, M., Roger, J. C., Dubuisson, P., Piazzola, J., and Despiau, S.: One year measurements of aerosol optical properties over an urban coastal site: effect on local direct radiative forcing, Atmos. Res., 90, 195–202, doi:10.1016/j.atmosres.2008.02.003, 2008.
Saha, S., Moorthi, S., Pan, H.-L., Wu, X., Wang, J., Nadiga, S., Tripp, P., Kistler, R., Woollen, J., Behringer, D., Liu, H., Stokes, D., Grumbine, R., Gayno, G., Wang, J., Hou, Y.-T., Chuang, H.-Y., Juang, H.-M. H., Sela, J., Iredell, M., Treadon, R., Kleist, D., Van Delst, P., Keyser, D., Derber, J., Ek, M., Meng, J., Wei, H., Yang, R., Lord, S., Van Den Dool, H., Kumar, A., Wang, W., Long, C., Chelliah, M., Xue, Y., Huang, B., Schemm, J.-K., Ebisuzaki, W., Lin, R., Xie, P., Chen, M., Zhou, S., Higgins, W., Zou, C.-Z., Liu, Q., Chen, Y., Han, Y., Cucurull, L., Reynolds, R. W., Rutledge, G., and Goldberg, M.: The NCEP climate forecast system reanalysis, B. Am. Meteorol. Soc., 91, 1015–1057, doi:10.1175/2010BAMS3001.1, 2010.
Saïd, F., Canut, G., Durand, P., Lohou, F., and Lothon, M.: Seasonal evolution of boundary-layer turbulence measured by aircraft during the AMMA 2006 Special Observation Period, Q. J. Roy. Meteor. Soc., 136, 47–65, doi:10.1002/qj.475, 2010.
Salvador, P., Alonso-Pérez, S., Pey, J., Artíñano, B., de Bustos, J. J., Alastuey, A., and Querol, X.: African dust outbreaks over the western Mediterranean Basin: 11 year characterization of atmospheric circulation patterns and dust source areas, Atmos. Chem. Phys., 14, 6759–6775, doi:10.5194/acp-14-6759-2014, 2014.

ACPD
15, 21607–21669, 2015

Scheuvens, D., Schütz, L., Kandler, K., Ebert, M., and Weinbruch, S.: Bulk composition of northern African dust and its source sediments – a compilation, Earth.-Sci. Rev., 116, 170–194, doi:10.1016/j.earscirev.2012.08.005, 2013.
Schladitz, A., Muller, T., Kaaden, N., Massling, A., Kandler, K., Ebert, M., Weinbruch, S., Deutscher, C., and Wiedensohler, A.: In situ measurements of optical properties at Tinfou (Morocco) during the Saharan mineral dust experiment samum 2006, Tellus B, 61, 64–78, doi:10.1111/j.1600-0889.2008.00397.x, 2009.
Schladitz, A., Müller, T., Nordmann, S., Tesche, M., Groß, S., Freudenthaler, V., Gasteiger, J., and Wiedensohler, A.: In situ aerosol characterization at Cape Verde, Tellus B, 63, 549–572, doi:10.1111/j.1600-0889.2011.00568.x, 2011.
Seinfeld, J. H. and Pandis, S. N.: Atmospheric Chemistry and Physics: From air pollution to climate change, section 5, John Wiley, New York, 714 pp., 1998.
Sicard, M., Mallet, M., García-Vizcaíno, D., Comerón, A., Rocadenbosch, F., Dubuisson, P., and Muñoz-Porcar, C.: Intense dust and extremely fresh biomass burning outbreak in Barcelona, Spain: characterization of their optical properties and estimation of their direct radiative forcing, Environ. Res. Lett., 7, 034016, doi:10.1088/1748-9326/7/3/034016, 2012.
Sicard, M., Bertolín, S., Mallet, M., Dubuisson, P., and Comerón, A.: Estimation of mineral dust long-wave radiative forcing: sensitivity study to particle properties and application to real cases in the region of Barcelona, Atmos. Chem. Phys., 14, 9213–9231, doi:10.5194/acp-14-9213-2014, 2014.
Skamarock, W. C., Klemp, J. B., Dudhia, J., Gill, D. O., Barker, D. M., Huang, X. Z., Wang, W., and Powers, J. G.: A Description of the Advanced Research WRF Version 3. Technical report, Mesoscale and Microscale Meteorology Division, NCAR, Boulder, Colorado, 2008.
Sokolik, I. N. and Toon, O. B.: Direct radiative forcing by anthropogenic airborne mineral aerosols, Nature, 381, 681–683, 1996.
Sullivan, A. P. and Weber, R. J.: Chemical characterization of the ambient organic aerosol soluble in water: 2. Isolation of acid, neutral, and basic fractions by modified size-exclusion chromatography, J. Geophys. Res., 111, D05315, doi:10.1029/2005JD006486, 2006.
Sullivan, R. C. and Prather, K. A.: Investigations of the diurnal cycle and mixing state of oxalic acid in individual particles in Asian aerosol outflow, Environ. Sci. Technol., 41, 8062–8069, doi:10.1021/es071134g, 2007.
Sullivan, R. C., Moore, M. J. K., Petters, M. D., Kreidenweis, S. M., Roberts, G. C., and Prather, K. A.: Effect of chemical mixing state on the hygroscopicity and cloud nucle-

ACPD
15, 21607–21669, 2015

ation properties of calcium mineral dust particles, Atmos. Chem. Phys., 9, 3303–3316, doi:10.5194/acp-9-3303-2009, 2009.
Swap, R., Garstang, M., Greco, S., Talbot, R., and Kållberg, P.: Saharan dust in the Amazon Basin, Tellus B, 44, 133–149, doi:10.1034/j.1600-0889.1992.t01-1-00005.x, 1992.
Tegen, I. and Lacis, A. A.: Modeling of particle size distribution and its influence on the radiative properties of mineral dust aerosol, J. Geophys. Res.-Atmos., 101, 19237–19244, doi:10.1029/95JD03610, 1996.
Trochkine, D., Iwasaka, Y., Matsuki, A., Yamada, M., Kim, Y. S., Nagatani, T., Zhang, D., Shi, G. Y., and Shen, Z.: Mineral aerosol particles collected in Dunhuang, China, and their comparison with chemically modified particles collected over Japan, J. Geophys. Res.-Atmos., 108, 8642, doi:10.1029/2002JD003268, 2003.
Tsyro, S., Simpson, D., Tarrasón, L., Klimont, Z., Kupiainen, K., Pio, C., and Yttri, K. E.: Modeling of elemental carbon over Europe, J. Geophys. Res.-Atmos., 112, D23S19, doi:10.1029/2006JD008164, 2007.
Ullerstam, M., Vogt, R., Langer, S., and Ljungstrom, E.: The kinetics and mechanism of SO_2 oxidation by O_3 on mineral dust, Phys. Chem. Chem. Phys., 4, 4694–4699, doi:10.1039/B203529B, 2002.
Valenzuela, A., Olmo, F. J., Lyamani, H., Granados-Muñoz, M. J., Antón, M., Guerrero-Rascado, J. L., Quirantes, A., Toledano, C., Perez-Ramírez, D., and Alados-Arboledas, L.: Aerosol transport over the Werstern Mediterranean bassin: evidence of fine particles to desert plumes over Alboran Island, J. Geophys. Res.-Atmos., 119, 14028–14044, doi:10.1002/2014JD022044, 2014.
Villani, P., Picard, D., Marchand, N., and Laj, P.: Design and Validation of a 6-Volatility Tandem Differential Mobility Analyzer (VTDMA), Aerosol Sci. Technol., 41, 898–906, doi:10.1080/02786820701534593, 2007.
Weinzierl, B., Petzold, A., Esselborn, M., Wirth, M., Rasp, K., Kandler, K., Schütz, L., Koepke, P., and Fiebig, M.: Airborne measurements of dust layer properties, particle size distribution and mixing state of Saharan dust during SAMUM 2006, Tellus B, 61, 96–117, doi:10.1111/j.1600-0889.2008.00392.x, 2009.
Weinzierl, B., Sauer, D., Esselborn, M., Petzold, A., Veira, A., Rose, M., Mund, S., Wirth, M., Ansmann, A., Tesche, M., Gross, S., and Freudenthaler, V.: Microphysical and optical properties of dust and tropical biomass burning aerosol layers in the Cape Verde region-an overview

ACPD
15, 21607–21669, 2015

of the airborne in situ and lidar measurements during SAMUM-2, Tellus B, 63, 589–618, doi:10.1111/j.1600-0889.2011.00566.x, 2011.

Wiedensohler, A., Birmili, W., Nowak, A., Sonntag, A., Weinhold, K., Merkel, M., Wehner, B., Tuch, T., Pfeifer, S., Fiebig, M., Fjäraa, A. M., Asmi, E., Sellegri, K., Depuy, R., Venzac, H., Villani, P., Laj, P., Aalto, P., Ogren, J. A., Swietlicki, E., Williams, P., Roldin, P., Quincey, P., Hüglin, C., Fierz-Schmidhauser, R., Gysel, M., Weingartner, E., Riccobono, F., Santos, S., Grüning, C., Faloon, K., Beddows, D., Harrison, R., Monahan, C., Jennings, S. G., O'Dowd, C. D., Marinoni, A., Horn, H.-G., Keck, L., Jiang, J., Scheckman, J., McMurry, P. H., Deng, Z., Zhao, C. S., Moerman, M., Henzing, B., de Leeuw, G., Löschau, G., and Bastian, S.: Mobility particle size spectrometers: harmonization of technical standards and data structure to facilitate high quality long-term observations of atmospheric particle number size distributions, Atmos. Meas. Tech., 5, 657–685, doi:10.5194/amt-5-657-2012, 2012.

Zhou, M., Okada, K., Qian, F., Wu, P. M., Su, L., Casareto, B. E., and Shimohara, T.: Characteristics of dust-storm particles and their long-range transport from China to Japan – case studies in April 1993, Atmos. Res., 40, 19–31, doi:10.1016/0169-8095(95)00023-2, 1996.

ACPD
15, 21607–21669, 2015

Table 1. Detailed information about the flights (number (ID), date, take-off time (TO), landing time (L) and route), the vertical profiles (latitude (Lat), longitude (Lon) and start time) and the dust layers sampled (height in meter, origin, age in day) during the ADRIMED airborne campaign. Times are expressed in Greenwich Mean Time (GMT).

Flight information					Vertical profile			Dust layer		
ID	Date	TO	L	Flight route	Lat	Lon	Start time	Height	Origin	Age
F29	16 June 2013	08:18	10:20	Cagliari – Minorca	40° N	5° E	09:50	2200–4500	southwestern Algeria	4.5
F30	16 June 2013	11:58	14:40	Minorca – Granada	37° N	4° W	14:20	2400–4800	southwestern Algeria	4
F31	17 June 2013	07:15	09:54	Granada – Minorca	37° N	4° W	07:15	2800–5400	southern Algeria	3.5
F32	17 June 2013	11:45	13:43	Minorca – Cagliari	40° N	5° E	11:45	1000–4600	southwestern Algeria	4.5
F33	19 June 2013	11:35	15:00	Cagliari – East Corsica	43° N	9° E	12:50	3000–4000	northeastern Algeria	2
								1500–3000	northeastern Algeria	3
F34	20 June 2013	11:00	14:15	Cagliari – West Corsica	43° N	7° E	12:20	> 2800	Tunisia	1
								1600–2800	Tunisia	5
F35	22 June 2013	08:47	11:26	Cagliari – Lampedusa	36° N	13° E	10:25	> 3500	southern Algeria	2
								1500–3500	southern Morocco	4
F38	28 June 2013	10:59	13:29	Cagliari – Lampedusa	36° N	13° E	12:30	1200–4500	Tunisia	3
F42	3 July 2013	08:29	11:55	Cagliari – Lampedusa	36° N	13° E	09:50	> 3000	Tunisia	3.5
								< 3000	southern Morocco	3.5

ACPD
15, 21607–21669, 2015

Table 2. Instruments detailed in this article operating onboard the ATR-42 aircraft during the ADRIMED campaign.

Parameter measured	Instrument	Abbreviation	Location in the aircraft	Wavelength (nm)	Nominal size range (µm)	Temporal resolution
Size distribution	Forward Scattering Spectrometer Probe, Model 300, Particle Measuring Systems	FSSP-300	wing-mounted	632.8	0.28–20	1 s
	Ultra High Sensitivity Aerosol Spectrometer, Droplet Measument Technologies	UHSAS	wing-mounted	1054	0.04–1	1 s
	Sky-Optical Particle Counter, Model 1.129, Grimm Technik	GRIMM	AVIRAD inlet	655	0.25–32	6 s
	Scanning mobility particle sizer, custom-built (Villani et al., 2007)	SMPS	community aerosol inlet	n/a	0.03–0.4	2 min
Integrated number concentration	Condensation Particle Counters, Model 3075, TSI	CPC	AVIRAD inlet	n/a	> 0.005	1 s
Chemical composition	Filter sampling	n/a	AVIRAD inlet	n/a	n/a	20–40 min
	Single particle soot photometer, Droplet Measurement Technologies	SP2	community aerosol inlet	1064	0.08–0.5	1 s
Scattering coefficient	3λ Integrated Nephelometer, Model 3563, TSI	Nephelometer	AVIRAD inlet	450, 550, 700	n/a	1 s
Extinction coefficient	Cavity Attenuated Phase Shift, Aerodyne Research Inc.	CAPS	community aerosol inlet	530	n/a	1 s

ACPD
15, 21607–21669, 2015

Table 3. Parameters (geometric median diameter $D_{p,g,i}$ in µm, standard deviation σ_i, and integrated number concentration $N_{tot,i}$ in $\#\,cm^{-3}$) of the four log-normal distributions used to parameterize the number size distributions obtained at the different altitudes. The mean, minimum and maximum of all parameters are listed.

		$D_{p,g,1}$	σ_1	$N_{tot,1}$	$D_{p,g,2}$	σ_2	$N_{tot,2}$	$D_{p,g,3}$	σ_3	$N_{tot,3}$	$D_{p,g,4}$	σ_4	$N_{tot,4}$
Elevated Dust layer	mean	0.08	1.25	170	0.12	1.60	300	0.32	1.70	15	1.3	2.2	3.0
	min	0.09	1.20	80.0	0.13	1.30	80.0	0.18	1.65	40	2.5	1.8	0.1
	max	0.08	1.25	320	0.12	1.56	600	0.32	1.70	45	1.3	2.2	12
Intermediate dust layer	mean	0.08	1.25	300	0.12	1.60	700	0.32	1.70	15	2.0	2.4	1.0
	min	0.08	1.25	250	0.11	1.50	400	0.20	1.70	35	1.7	2.1	0.7
	max	0.08	1.25	600	0.13	1.50	1100	0.18	1.90	80	1.7	2.0	2.5
Boundary layer	mean	0.08	1.25	450	0.12	1.60	650	0.32	1.70	5.0	1.3	2.1	1.0
	min	0.08	1.25	150	0.12	1.60	200	0.30	1.70	1.8	1.0	2.1	0.1
	max	0.08	1.25	600	0.12	1.60	1400	0.32	1.70	15	1.3	2.1	3.0

ACPD
15, 21607–21669, 2015

Table 4. Optical parameters (real part of the complex refractive index n_r, imaginary part of the complex refractive index n_i, single scattering albedo ω_0, asymmetry parameter g and mass extinction efficiency k_{ext}) all at $\lambda = 530$ nm as a function of the altitude. The mean, minimum and maximum of all parameters are listed.

		n_r	n_i	ω_0	g	k_{ext}
Elevated dust layer	mean	1.53	0.003	0.95	0.8	0.4
	min	1.50	0.000	0.90	0.7	0.3
	max	1.55	0.005	1.00	0.8	0.5
Intermediate dust layer	mean	1.52	0.003	0.94	0.7	0.5
	min	1.50	0.000	0.90	0.6	0.4
	max	1.55	0.005	1.00	0.7	0.7

ACPD
15, 21607–21669, 2015

Table 5. Concentrations of major crustal (Si, Al, Fe and Ca, in ng m^{-3}) and metallic tracers (Si, V, Pb and Zn, in ng m^{-3}), ionic species (SO_4^{2-}, NO_3^{2-}, NH_4^+, in ng m^{-3}), black carbon (in ng m^{-3}), mineral dust (in µg m^{-3}) and integrated fine mode of particles (in # cm^{-3}) during the ADRIMED airborne campaign. Dash indicates that the specie concentration was lower than the detection limit. The dust mass concentration was estimated from the measured Al using the mean Al mass fraction in the crustal composition of 7.09 % (Guieu et al., 2002). A comparison of the single scattering albedos ω_0 measured by the nephelometer and CAPS with those estimated from chemical measurements is also shown. The absolute error associated with ω_0 obtained from measurements is 0.04.

Flight number	F29	F30	F31	F32	F33	F34	F35	F38	F42
Si	3607	4955	4159	592	2426	9814	6430	2040	5366
Al	1404	2028	1719	225	975	3770	2519	746	2146
Fe	687	1085	845	146	536	1869	1239	416	1032
Ca	1099	1596	1547	–	1322	6404	2112	1374	1592
V	9	6	5	17	16	22	19	13	–
Pb	82	458	28	216	417	–	762	–	–
Zn	20	34	25	4	–	–	71	–	–
SO_4^{2-}	–	1740	–	2016	1574	2505	966	1764	2011
NO_3^-	–	–	–	206	–	285	309	–	467
NH_4^+	–	809	276	640	563	613	–	557	–
rBC	62	97	64	130	57	97	37	97	78
Dust	15.1	21.7	18.4	2.4	10.5	40.5	27.0	8.0	23.0
N_{fine}	316	416	457	881	515	988	229	485	714
ω_0 (measured)	0.97	1.00	0.99	0.92	0.98	0.94	0.97	0.94	0.99
ω_0 (chemistry)	0.93	0.96	0.95	0.94	0.96	0.96	0.97	0.94	0.96

ACPD
15, 21607–21669, 2015

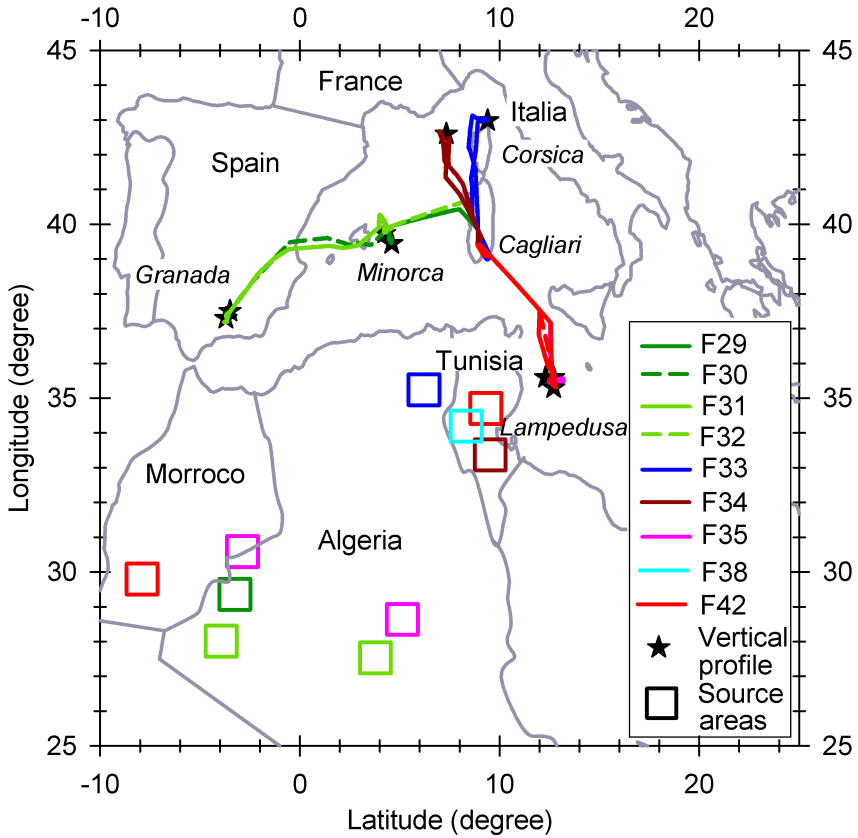

Figure 1. Operating region of the ATR-42 aircraft during the ADRIMED flights that performed mineral dust measurements. Colors of the lines and squares correspond to the different flights. The positions of the middle of the profiles are shown in black stars. Squares indicate likely sources regions of the dust sampled during the flights. The aircraft was based at Cagliari in Sardinia.

ACPD
15, 21607–21669, 2015

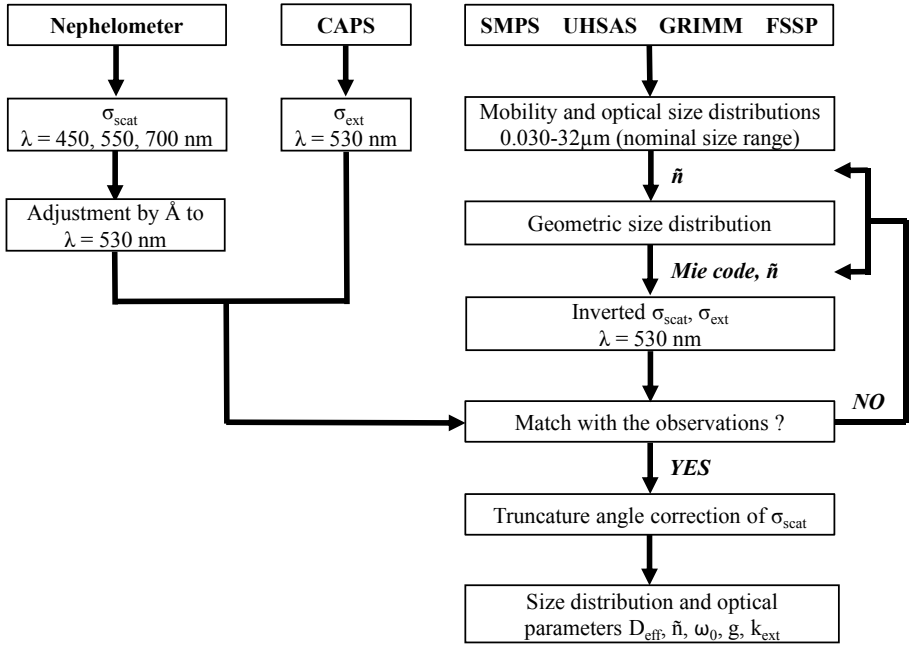

Figure 2. Data inversion procedure to retrieve the dust size distribution and optical parameters.

ACPD
15, 21607–21669, 2015

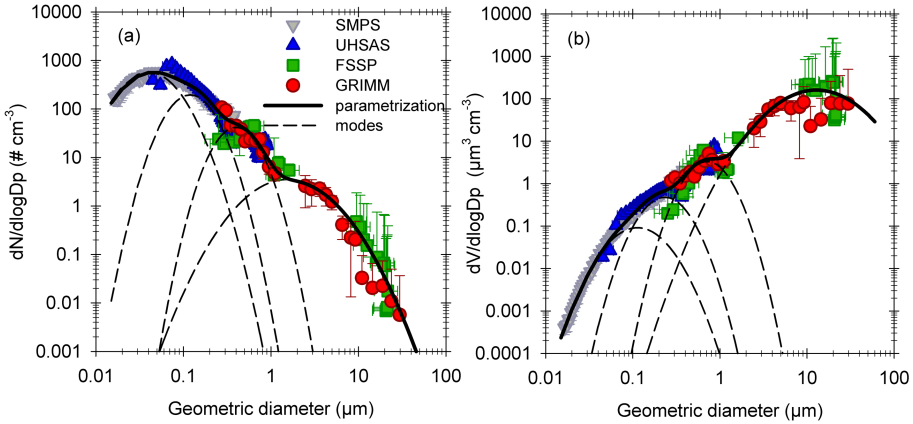

Figure 3. Number **(a)** and volume **(b)** size distributions obtained by the SMPS (gray), UHSAS (blue), FSSP (green) and GRIMM (red) during the flight F35 including refractive index corrections for $\tilde{n} = 1.53–0.004i$. Vertical errors bars indicate one standard deviation of the data during the straight levelled run. The dark line represents the parametrized fit with a sum of four log-normal modes (shown in dashed lines).

ACPD
15, 21607–21669, 2015

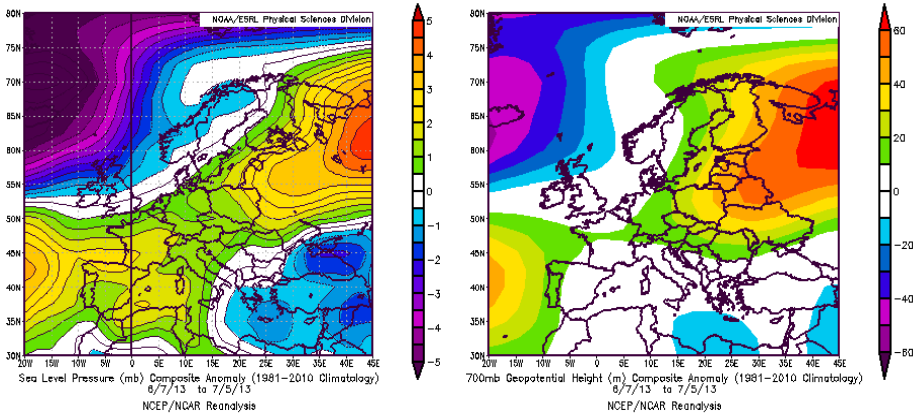

Figure 4. Sea level pressure in hPa (left) and 700 hPa geopotential height in m (right) composite anomalies with respect to the 1981–2010 climatology obtained from the NCEP/NCAR Reanalysis (images provided by the NOAA/ESRL Physical Sciences Division, Boulder Colorado, from their web site at http://www.esrl.noaa.gov/psd/).

ACPD
15, 21607–21669, 2015

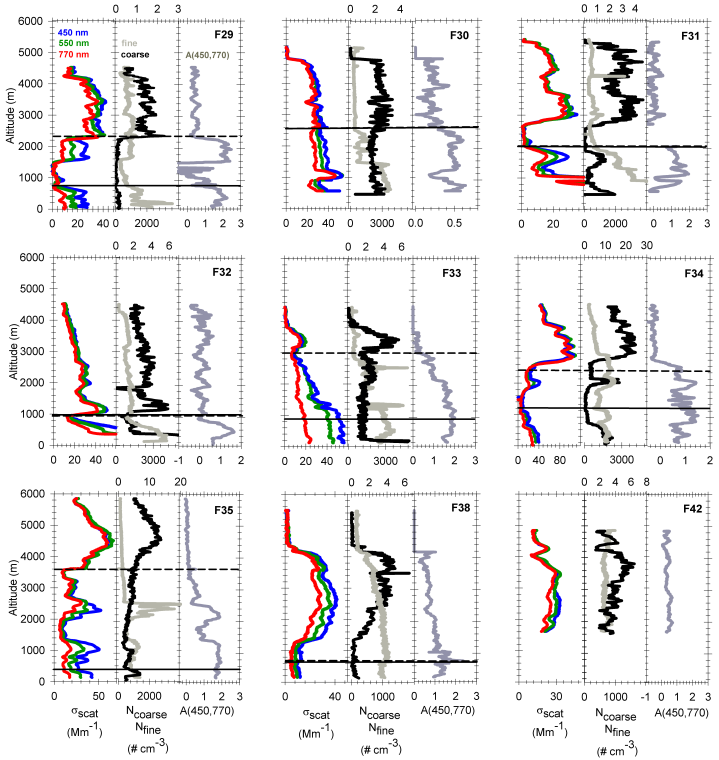

Figure 5. Vertical profiles of the spectral scattering coefficient σ_{scat} at λ = 450, 550 and 770 nm (blue, green and red), the particle number concentration in the submicron N_{fine} (light grey) and the supermicron N_{coarse} (dark) size ranges and the scattering Angstrom exponent Å calculated between 450 and 770 nm (dark grey). N_{coarse} is plotted using the upper horizontal axis. The top of the boundary layer Z_b and the wind shear level Z_s are indicated in line and in dashed line respectively. The heights of Z_b and Z_s were situated below the minimum flight level in F42. Data were corrected for Standard Temperature and Pressure (STP) using T = 20 °C and P = 1013.25 hPa.

ACPD
15, 21607–21669, 2015

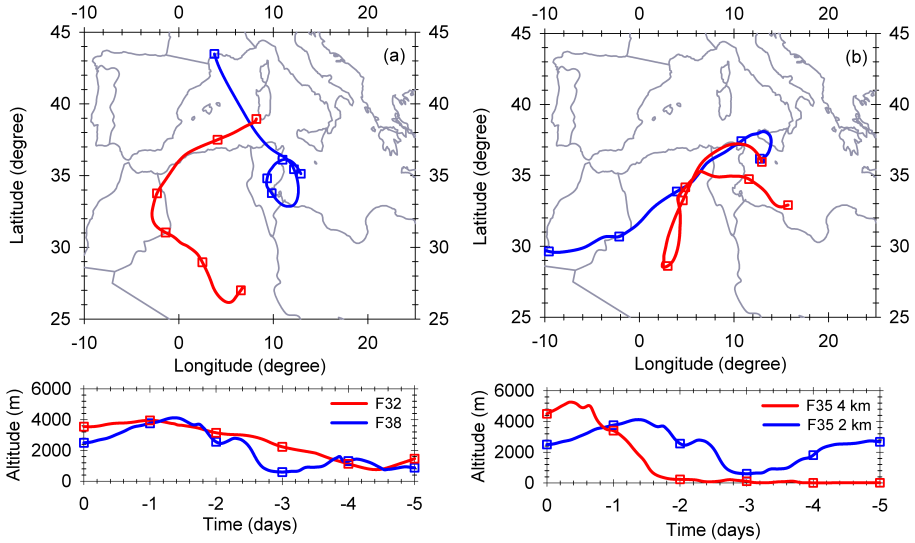

Figure 6. Five-day backward trajectories calculated for **(a)** flights F32 and F38 and **(b)** flight F35 arriving at intermediate (2 km a.s.l.) and elevated (4 km a.s.l.) altitudes in blue and red, respectively.

ACPD
15, 21607–21669, 2015

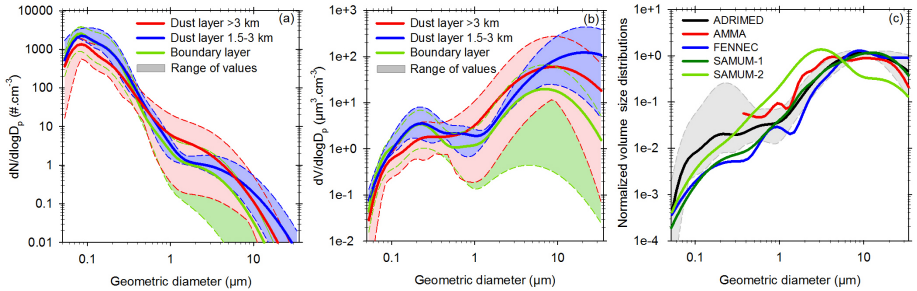

Figure 7. Particle size distributions obtained in the dust layers during ADRIMED for **(a)** number distribution, **(b)** volume distribution and **(c)** volume distribution normalized by the total volume concentration. In Figures **(a)** and **(b)**, size distributions are classified as a function of the altitude of the layer: elevated dust layer above 3 km a.s.l. (red), intermediate dust layer between 1.5–3 km a.s.l. (blue) and the boundary layer below 1 km (green). The shading represents the minimum and maximum throughout the campaign. In Figure **(c)**, the mean (dark line), minimum and maximum normalized size distributions (grey shading) observed above 1.5 km during the ADRIMED campaign are compared with those observed in the source region during the airborne campaigns AMMA (red line, Formenti et al., 2011a), FENNEC (blue line, Ryder et al., 2013b) and SAMUM1 (dark green line, Weinzierl et al., 2009), as well as with measurements at Cape-Verde region during SAMUM-2 campaign (light green line, Weinzierl et al., 2011). The AMMA curve (Formenti et al., 2011) is curtailed to 0.3 µm since there was no measurement below this size during the campaign.

ACPD
15, 21607–21669, 2015

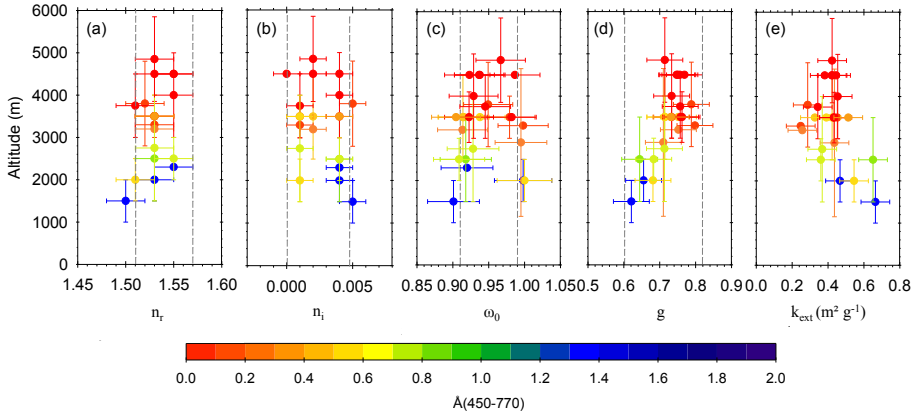

Figure 8. Scatter plots showing **(a)** the real part of the complex refractive index, **(b)** the imaginary part of the complex refractive index, **(c)** the single scattering albedo, **(d)** the asymmetry parameter and **(e)** the mass extinction efficiency all at $\lambda = 530$ nm as a function of the altitude from all straight level runs and vertical profiles within the dust layers measured during the campaign. The altitude indicated for vertical profiles refers to the middle of the layer. Dashed lines indicate the range of values obtained in dust source regions. The maximum value of k_{ext} reported in the literature for dust in source regions is above 0.8 m^2 g^{-1}.

ACPD
15, 21607–21669, 2015

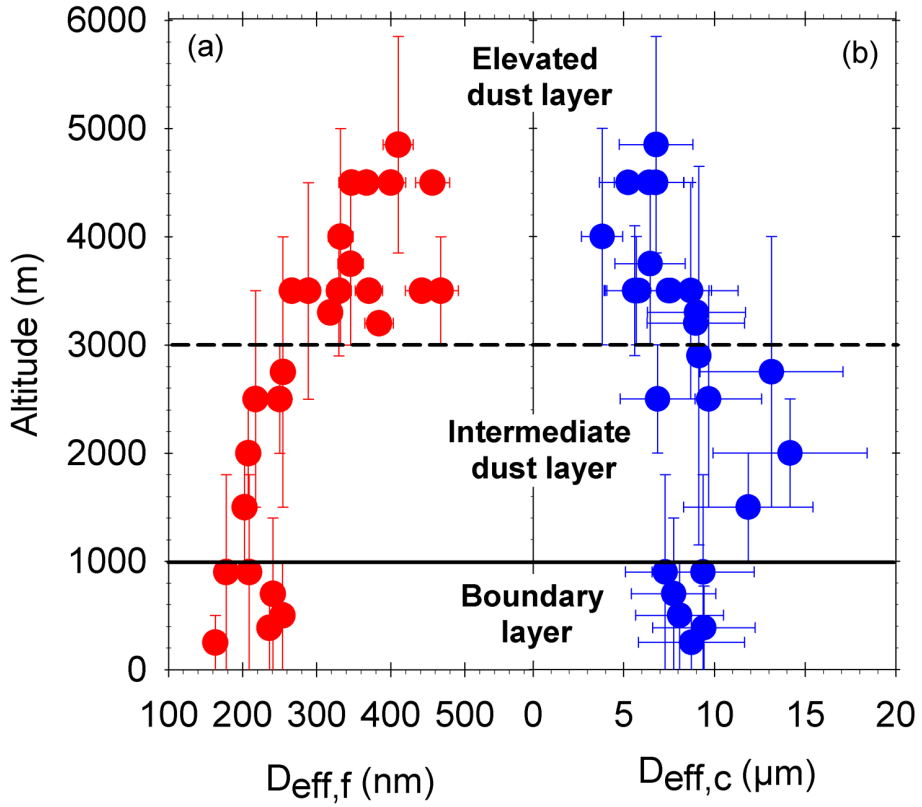

Figure 9. Altitude dependence of **(a)** the fine mode effective diameter $D_{eff,f}$ (size range 0.053–1 μm) and **(b)** the coarse mode effective diameter $D_{eff,c}$ (size range 1–32 μm). The altitude reported for vertical profiles refers to the middle of the layer. Broad classifications of the elevated dust layer, the intermediate dust layer and the boundary layer have been added to the figure.

ACPD
15, 21607–21669, 2015

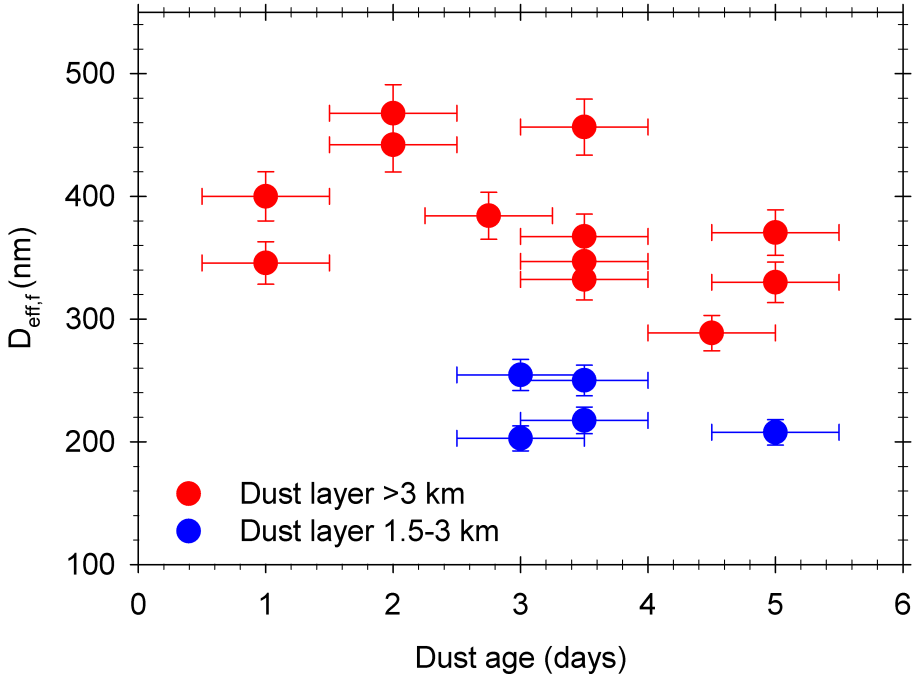

Figure 10. Effective diameter of the fine mode $D_{eff,f}$ as a function of the dust age observed for elevated dust layers (red circles) and intermediate dust layers (blue circles).

ACPD
15, 21607–21669, 2015

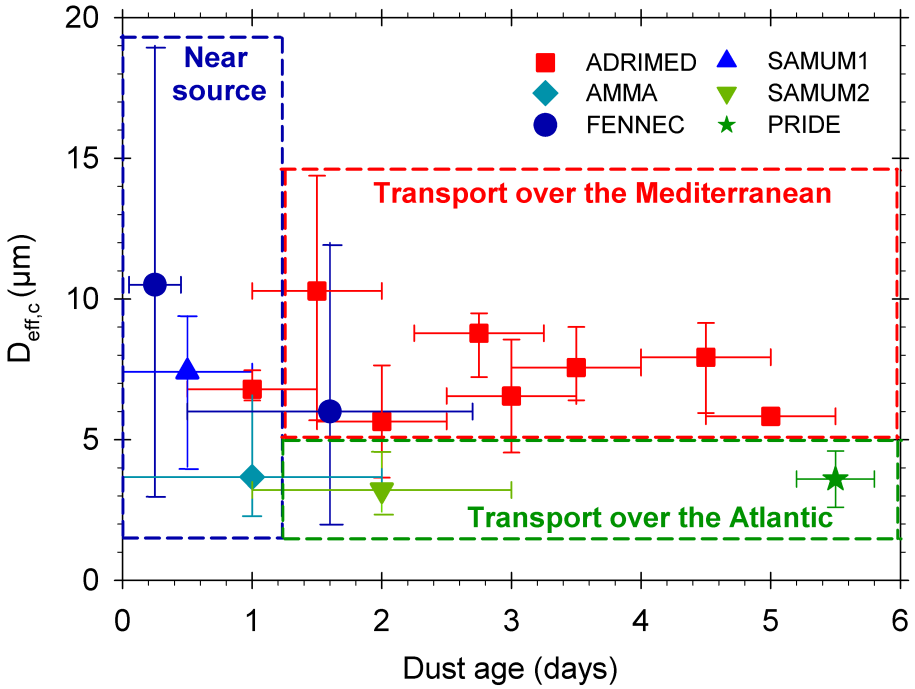

Figure 11. Effective diameter of the coarse mode $D_{eff,c}$ as a function of the dust age observed during ADRIMED (red squares). Values are compared to those observed in dust source region (in blue) during FENNEC (circles), SAMUM1 (triangle) and AMMA (diamond), as well as measurements in the Atlantic Ocean (in green) at Cape-Verde region during SAMUM-2 (triangle) and at Puerto-Rico during PRIDE (stars). The horizontal error bars represent uncertainties on the dust age estimated using HYSPLIT and Seviri RGB images. The vertical error bars represent the range of values obtained for each dust age.

ACPD
15, 21607–21669, 2015

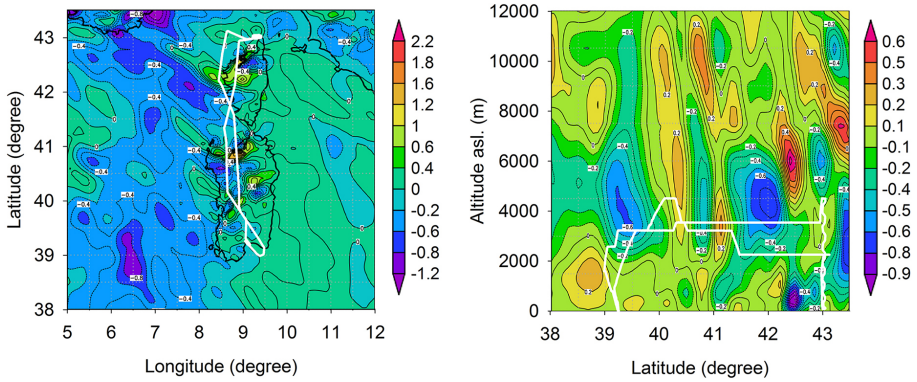

Figure 12. 700 hPa vertical velocity field **(a)** and vertical cross section **(b)**, taken along the F33 flight track (white line), from the 10 km resolution WRF model simulations. Values are expressed in $Pa\,s^{-1}$.

ACPD
15, 21607–21669, 2015